A 6 year record of baroclinic transport variability of the Antarctic Circumpolar Current at 140°E derived from expendable bathythermograph and altimeter measurements

Stephen R. Rintoul, Serguei Sokolov, and John Church

Antarctic Cooperative Research Centre and CSIRO Marine Research, Hobart, Tasmania, Australia

Received 8 January 2001; revised 7 September 2001; accepted 26 September 2001; published 17 October 2002.

[1] Repeat hydrographic sections across the Antarctic Circumpolar Current are used to derive an empirical relationship between upper ocean temperature and the baroclinic transport stream function. Cross validation shows this relationship can be used to infer baroclinic transport (above and relative to 2500 dbar) from temperature measurements with an error of a few per cent. The mean transport distribution derived from 31 austral summer expendable bathythermograph (XBT) sections over a 6 year period consists of westward flow immediately south of Tasmania, a broad band of strong eastward flow between 50° and 55°S, and three cores of eastward flow south of 55°S. By defining a second empirical relationship between surface dynamic height and cumulative transport a continuous time series of baroclinic transport is derived from altimeter measurements of sea surface height. Transports derived from altimetry in this way agree well with simultaneous in situ estimates (root mean square error in net transport is 4×10^6 m^3 s^{-1}), suggesting sea level anomalies largely reflect baroclinic changes above 2500 dbar. The 10 day sampling of the altimeter transport time series shows the irregular XBT sampling aliases variability at unresolved timescales. The standard deviation of net transport above and relative to 2500 m is 4.3×10^6 m^3 s^{-1}. The variability in net transport is largest (2.7×10^6 m^3 s^{-1}) in the quasi-annual band (periods of 4 months to 1.5 years), slightly smaller (2.3×10^6 m^3 s^{-1}) in the mesoscale band (<4 months), and smallest in the interannual band (>1.5 years, 1.5×10^6 m^3 s^{-1}). Changes in transport are correlated with local changes in both wind stress and wind stress curl in the quasi-annual and interannual bands, but the transport time series is too short to draw significant conclusions. *INDEX TERMS:* 4207 Oceanography: General: Arctic and Antarctic oceanography; 4215 Oceanography: General: Climate and interannual variability (3309); 4512 Oceanography: Physical: Currents; 4528 Oceanography: Physical: Fronts and jets; 4227 Oceanography: General: Diurnal, seasonal, and annual cycles; *KEYWORDS:* baroclinic transport; Antarctic Circumpolar Current; interannual variability; satellite altimeter; XBT

Citation: Rintoul, S. R., S. Sokolov, and J. Church, A 6 year record of baroclinic transport variability of the Antarctic Circumpolar Current at 140°E derived from expendable bathythermograph and altimeter measurements, *J. Geophys. Res.*, *107*(C10), 3155, doi:10.1029/2001JC000787, 2002.

1. Introduction

[2] The Antarctic Circumpolar Current (ACC) provides the primary means of exchange between the ocean basins. The interbasin exchange accomplished by the ACC is an important link in the global overturning circulation [*Schmitz*, 1995, 1996] and also allows anomalies such as the Antarctic Circumpolar Wave [*White and Peterson*, 1996] to propagate from one basin to another. The ACC therefore has an impact on both global [e.g., *Rintoul et al.*, 2001] and regional climate [*White and Cherry*, 1998; *White*, 2000]. As a result, the transport of the ACC has been a topic of intense oceanographic interest for many years.

[3] However, our understanding of how and why the ACC transport varies with time is incomplete, largely due to the lack of observations. Measurements in Drake Passage during the International Southern Ocean Studies (ISOS) program in the 1970's provided the first estimates of ACC transport and variability [*Whitworth*, 1983; *Whitworth and Peterson*, 1985]. During the World Ocean Circulation Experiment (WOCE), measurements were made at a number of locations in the Southern Ocean. Repeat sections from which transport variability could be assessed were limited to the three "chokepoints" between Antarctica and the southern hemisphere continents. *Rintoul and Sokolov* [2001] describe the variability in baroclinic property transports based on six occupations of the WOCE repeat hydrographic section (SR3) across the Australian "chokepoint". Here we present a more complete time series of upper ocean transport based on 45 austral summer expendable bathythermograph (XBT) sections collected between 1993 and 1999.

0148-0227/02/2001JC000787

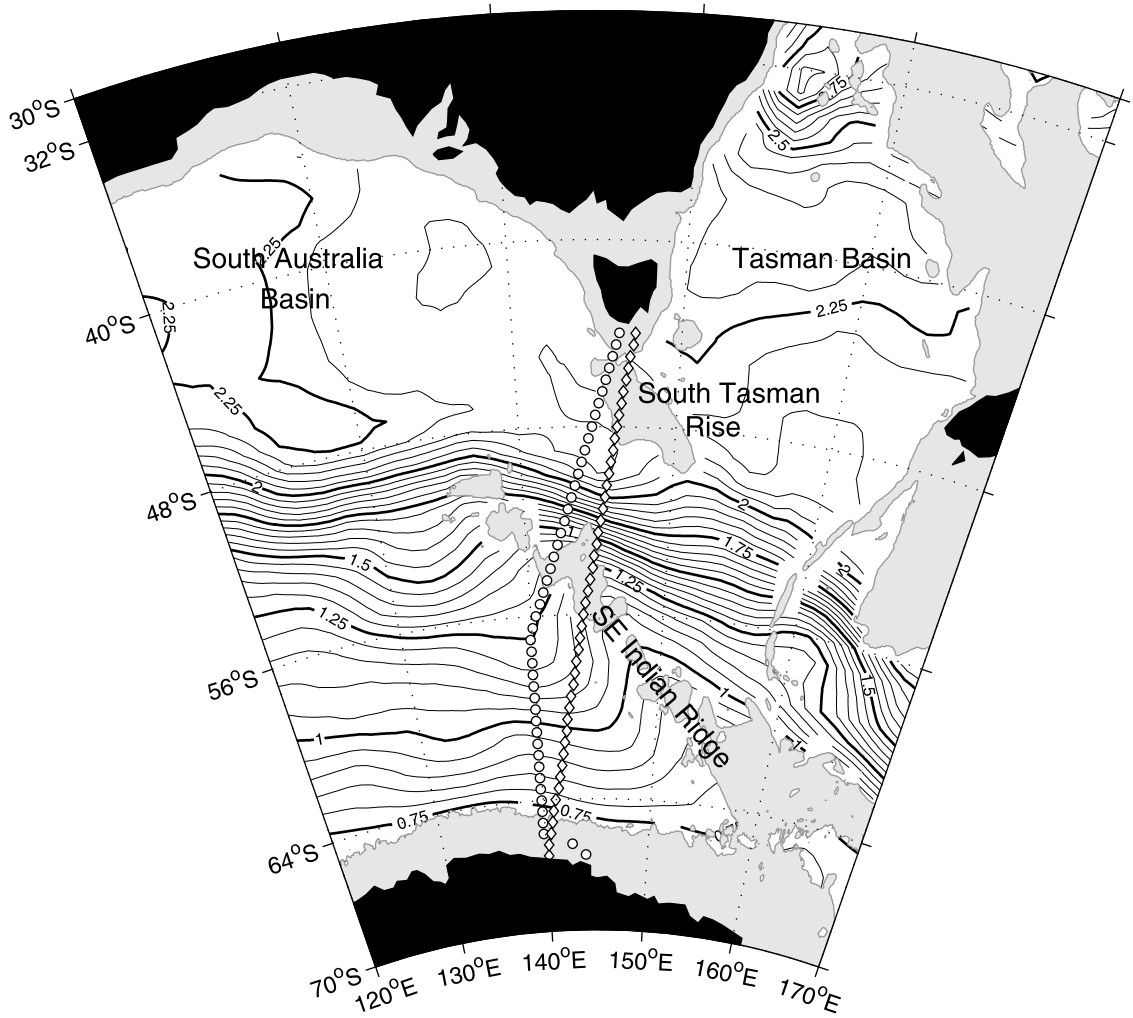

Figure 1. Location of WOCE repeat section SR3 (dots) and the high density repeat XBT line IX28 (diamonds) carried out by the SURVOSTRAL program. The contours show the dynamic height (in dyn m) at the sea surface relative to 2500 m from the climatology of *Olbers et al.* [1992]. Depths less than 3000 m depth are shaded.

[4] To estimate baroclinic transport from XBT temperature measurements, some relationship between temperature and salinity must be assumed. Most commonly, a mean $T - S$ curve is determined for a region, allowing the salinity corresponding to a particular temperature to be found. Density, dynamic height, and velocities can then be calculated in the usual manner [e.g., *Stommel*, 1947]. In the Southern Ocean, a "tight" $T - S$ curve does not exist. Temperature and salinity profiles generally cool and freshen to the south, and at some locations the relationship is multivalued: one temperature corresponds to several salinity values. However, the $T - S$ curve is "stable" in the sense that the envelope of $T - S$ curves does not change with time, and each streamline is associated with a particular $T - S$ curve. We exploit this stability to derive a relationship between upper ocean temperature and the potential energy anomaly, or baroclinic transport stream function. The empirical relationship is used to infer baroclinic transport from summer XBT measurements obtained between 1993 and 1999.

[5] The XBT sections are collected from an Antarctic resupply ship which operates only in austral summer. The XBT time series therefore may alias variability at unresolved frequencies. To examine this possibility, we use satellite altimeter measurements of sea surface height to estimate baroclinic transport every 10 days. The technique is analogous to that used to derive transports from XBT data, except in this case we use CTD measurements to derive a relationship between surface dynamic height and baroclinic transport. We show that the transport estimates derived from both the XBT and altimeter data are accurate to within a few per cent. We find that the summer-only sampling of the XBT sections does indeed appear to alias transport variability at unresolved frequencies. The continuous six year baroclinic transport record derived from altimetry, while still short, is the first of sufficient duration and continuity to allow the timescales of ACC variability to be examined.

2. Data

[6] The locations of the repeat CTD and XBT sections south of Tasmania are shown in Figure 1. The CTD line, WOCE section SR3, has been repeated six times between 1991 and 1996, with at least one section in each season of

the year [*Rintoul and Sokolov*, 2001]. The usual station spacing on the CTD sections is 56 km, with tighter spacing across the sharp fronts of the ACC and over steeply sloping bathymetry. All stations reached to within about 10 m of the seafloor. Data processing details are described in a series of technical reports [*Rosenberg et al.*, 1995a, 1995b, 1996, 1997]. A discussion of the major circulation features and water masses along the SR3 section can be found in *Rintoul and Bullister* [1999] and *Rintoul and Sokolov* [2001].

[7] The XBT section has been occupied six or more times each austral summer since 1992 as part of the joint Australia-France-USA SURVOSTRAL program [*Rintoul et al.*, 1997]. The SURVOSTRAL program is conducted from the French Antarctic supply ship Astrolabe, and the sampling schedule is set by requirements to resupply the Antarctic base Dumont d'Urville. The first section each season is usually occupied in late October, and the last in early March, so the measurements span about five months of the year. A total of 45 XBT sections were occupied between December 1992 and March 1999. The typical station spacing is 37 km, with 19 km spacing across the ACC fronts, although extreme weather occasionally causes gaps in the sections. Temperature is measured to 800 m and a thermosalinograph measures surface temperature and salinity continuously along the cruise track. The XBT and CTD sections do not follow exactly the same cruise track: the separation at the northern end is about 80 km and the maximum separation between the two sections along a latitude circle is about 200 km at 57°S (Figure 1).

[8] We also estimate baroclinic transport from satellite altimeter measurements of sea surface height. We use the "Mean Sea Level Anomaly (MSLA)" product from CLS/AVISO, which provides sea level anomalies every 10 days mapped on a 1/4° grid using the TOPEX/Poseidon, ERS-1 and ERS-2 altimeters [*Le Traon et al.*, 1998]. *Ducet et al.* [2000] show that the gridded product is able to recover signals with wavelengths larger than 150 to 200 km in all directions. Details of the error corrections applied and mapping method can be found in the above references. Note that during the period December 24 1993 to March 24 1995 the maps use data from the TOPEX/Poseidon altimeter only.

[9] The mean dynamic topography from [*Olbers et al.*, 1992] is shown in Figure 1. The strongest part of the ACC lies on the northern flank of the Southeast Indian Ridge. Near 140°E the ridge and the current both turn to the southeast. Southern streamlines of the ACC, associated with the Polar Front and southern ACC front [*Orsi et al.*, 1995], turn north upon encountering the ridge, as expected for a deep-reaching flow conserving its planetary vorticity. After crossing the ridge, these streamlines turn back to the southeast.

3. Results

3.1. Full Depth Temperature Structure

[10] The potential temperature structure between Tasmania and Antarctica is illustrated in Figure 2, which shows a full depth section from a winter (September 1996) occupation of SR3. While the focus in this paper is on the repeat XBT line, Figure 2 shows how the upper ocean temperature structure is related to the deep ocean; this winter section also provides a useful comparison to the austral summer XBT data.

[11] A number of fronts are evident, which reach from the sea surface to the seafloor. In particular, isotherms slope up to the south between 50° and 53°S, associated with the Subantarctic Front (SAF), the strongest core of the ACC at this longitude. The SAF itself consists of a number of filaments at 51°S (stations 42 to 43), 52°S (stations 38 to 40), and 53°S (stations 35–36). *Rintoul and Sokolov* [2001] show that the SAF at the SR3 section is often observed to contain multiple bands of enhanced horizontal gradient of temperature and density (hence multiple geostrophic velocity maxima). A doming of the isotherms at 49°S (station 55) is associated with a meander or eddy of the SAF. The Polar Front (PF), defined as the northernmost extent of temperature minimum water cooler than 2°C at 200 m depth [*Botnikov*, 1963] lies between stations 32 and 33 at 54°S.

[12] Between the PF and 59°S, deep isotherms slope up gently to the north on the southern side of the Southeast Indian Ridge. Deep-reaching fronts occur near 59.5°, 62°, and 64°S. These fronts correspond to the southern branch of the PF [*Rintoul and Bullister*, 1999], the southern ACC front, and the southern boundary of the ACC, respectively [*Orsi et al.*, 1995]. *Rintoul and Sokolov* [2001] describe the transport variability of each of the fronts observed on six occupations of the SR3 line.

[13] Also shown in Figure 2 is the average temperature between 600 and 700 m ($\overline{T}_{650}$). It is clear that changes in $\overline{T}_{650}$ along the section are closely related to the major fronts evident in the temperature section. We exploit this correlation to infer transports in the upper 2500 dbar from upper ocean temperatures.

3.2. Examples of Upper Ocean Temperature Variability

[14] Upper ocean temperature along the SURVOSTRAL XBT line is generally similar to that of SR3, but with some significant differences. A time sequence of six sections from the 1994–1995 season illustrates the seasonal evolution of upper ocean temperature. The sequence begins in early November. Figure 3a looks similar to Figure 2, in the sense that there is no evidence of a warm summer mixed layer. This demonstrates that the sequence of XBT sections obtained each "austral summer" field season begins with characteristics typical of late winter or early spring.

[15] The mixed layer warms throughout the summer season, forming a seasonal thermocline at about 100 m depth across most of the section by early March (Figure 3f). The seasonal thermocline is particularly sharp south 55°S, where temperature decreases from about 3°C in the summer mixed layer to about 0.5°C in the remnant winter water over a depth interval of 10 to 20 m. Note that the temperature minimum layer extends further north on the SURVOSTRAL section than on SR3: for example, temperature minimum water cooler than 0°C extends to 54°S on the XBT line, and only to 59°S on SR3. This difference between the two lines is consistent with the northward deflection of dynamic height contours on the southern half of the sections seen in Figure 1.

[16] The SAF appears as a region of strong horizontal gradient near 51°S in each of the XBT sections. The width and latitude of the SAF vary somewhat from section to section (e.g., narrow in November (Figure 3a), broader in December (Figure 3c); note that the very broad front in Figure 3d is an artifact of the large gap in the station spacing on this section). In this particular year, the structure of the SAF is simpler than the multiple jets observed on SR3 in September 1996 (Figure 2). However, in other years, the

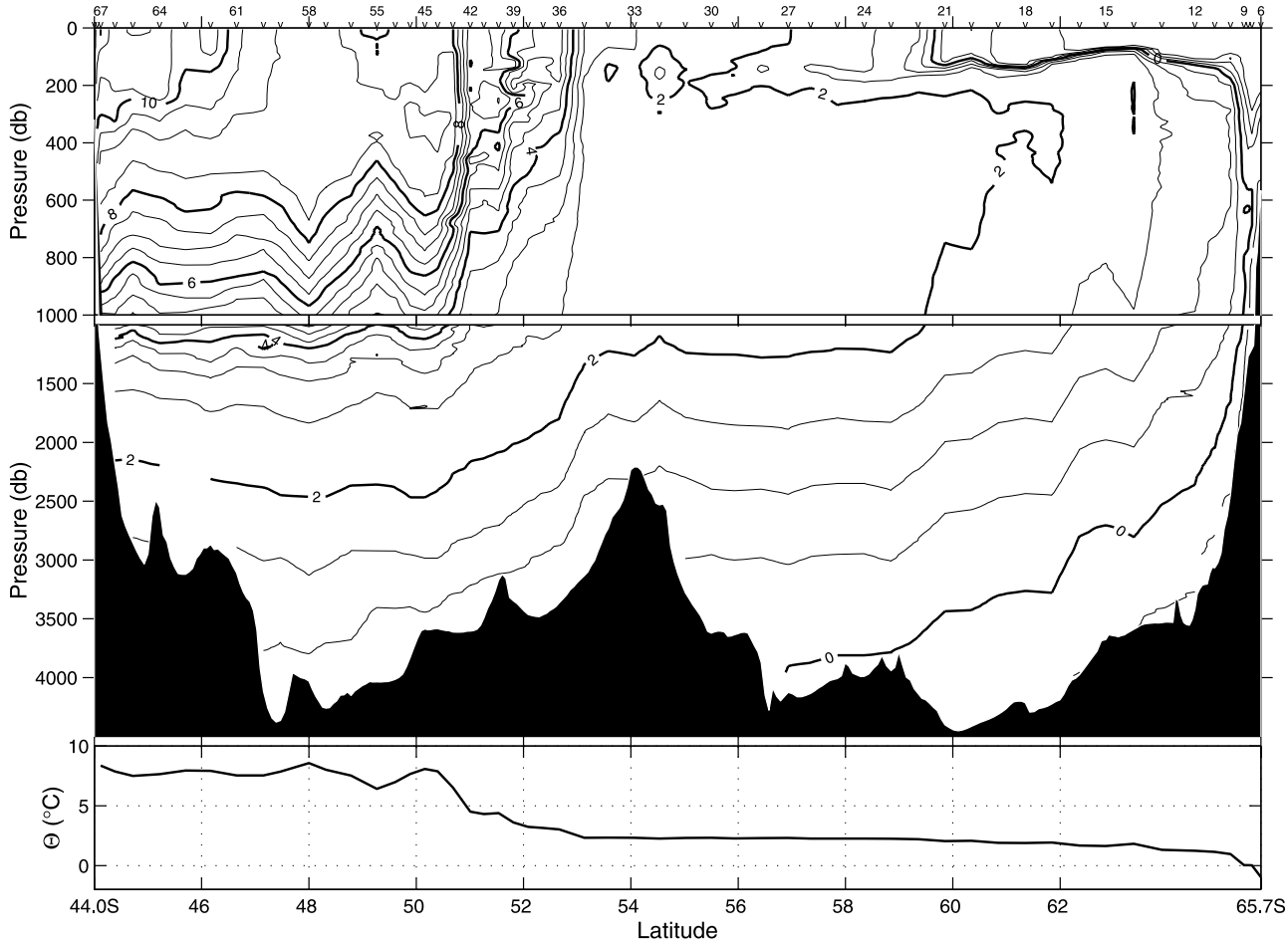

Figure 2. Potential temperature (°C) along the WOCE SR3 line in September 1996, with an expanded scale in the upper 1000 m. The contour interval is 0.5°C. Potential temperature averaged in the layer 600–700 m is shown in the lower panel.

SAF also appears to split at the SURVOSTRAL section. The northern branch of the PF (defined by the northernmost extent of temperature minimum water cooler than 2°C) is at times distinct from the SAF (e.g., Figure 3a) and at times merges with the SAF (e.g., Figure 3c). A common feature of the XBT sections is a cold core ring or meander in the subantarctic zone (e.g., near 48°S in Figure 3a): of 32 sections with sufficient resolution to say whether a cold core feature is present, 28 (88%) have at least a weak eddy/meander; 19 of the 32 (60%) have a strong feature.

3.3. Transports From XBT Data

[17] Many regions of the ocean are characterized by a tight temperature-salinity ($T - S$) relationship which can be exploited to determine geostrophic velocities from temperature observations alone: the salinity corresponding to the observed temperature is obtained from the $T - S$ curve, and density and dynamic height are calculated from the observed T and inferred S [*Stommel*, 1957]. In the Southern Ocean the $T - S$ curve is not "tight" in the sense of providing a one-to-one relationship between T and S. A particular temperature value may correspond to a wide range of salinity values [e.g., *Rintoul and Bullister*, 1999, Figure 3]. Nevertheless, the $T - S$ curves in the Southern Ocean are stable: each front, and each of the zones between the fronts, has a characteristic family of $T - S$ curves which does not change with time. This stability of the $T - S$ curve can be exploited by generalizing the technique of inferring S from observed T as commonly used in lower latitudes. (See *Watts et al.* [2001] for an alternative technique especially suited to inference of profile information from vertical integral measurements, such as acoustic travel time measured by inverted echo sounders.)

[18] One way to exploit the "stability" of the $T - S$ curve is to take advantage of correlations between observed temperature and dynamical quantities of interest. For example, *Rintoul et al.* [1997] showed that there was a tight relationship between temperature (averaged between 0 and 600 m) and dynamic height (at the sea surface relative to 2000 m) along the WOCE SR3 line. They used this empirical relationship to determine 0–2000 m dynamic heights from XBT measurements along the SURVOSTRAL track.

[19] Here our interest is in transport, and so we define a new empirical relationship between temperature, T, and the potential energy anomaly, χ, which is a stream function for the baroclinic transport.

$$\chi(p_o) = \frac{1}{g}\int_0^{p_o} p\delta dp; \tag{1}$$

$$U(p_o) = -\frac{1}{\rho_o f}\chi(p_o), \quad V(p_o) = \frac{1}{\rho_o f}\chi(p_o) \tag{2}$$

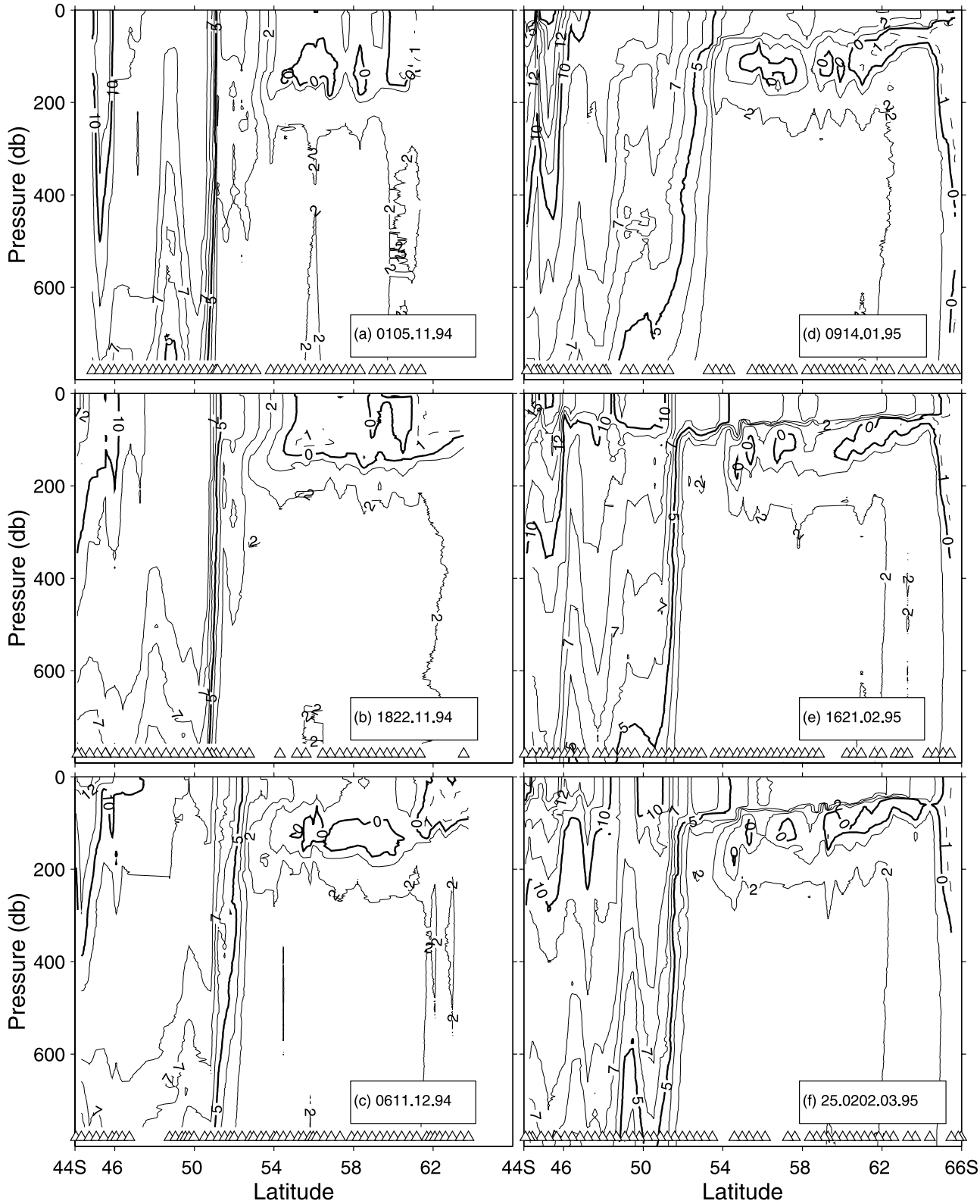

Figure 3. Evolution of upper ocean temperatures along the SURVOSTRAL XBT line during the 1994–1995 austral summer (early November to early March). Triangles indicate station positions. The contour interval is 1°C; the 0, 5, and 10°C contours are bold; and the −1°C contour is dashed.

Table 1. Baroclinic Volume Transport Above and Relative to 2500 dbar (U_{2500}, in Sv), on Six Occupations of the WOCE SR3 Line[a]

Cruise	Dates	U_{2500}, Sv	U_{2500}/U_{dcd}, %	U_{2500}/U_{bg}, %
AU9101	Oct, 1991	107.6	67.4	72.1
AU9309	Mar, 1993	96.9	66.6	71.0
AU9407	Jan, 1994	107.6	65.4	72.3
AU9404	Jan, 1995	97.7	65.5	72.3
AU9501	Jul, 1995	114.2	67.8	72.2
AU9601	Sep, 1996	111.7	61.9	71.6
mean ± s.d.			65.8 ± 2.1	71.9 ± 0.5

[a] The fourth and fifth columns give the ratio of the transport above and relative to 2500 dbar to the total baroclinic volume transport across SR3, relative to either the deepest common depth (U_{dcd}, column 4) or the "best guess" reference level described by *Rintoul and Sokolov* [2001] (U_{bg}, column 5).

where δ is the specific volume anomaly, g is gravity, p is pressure, p_o and ρ_o are the reference pressure and density respectively, and $U(V)$ is the zonal (meridional) geostrophic volume transport per unit width, above and relative to p_0. In the following, we use χ integrated to 2500 dbar (χ_{2500}). We use 2500 dbar because it is the deepest depth which still lies above the height of the mid-ocean ridge, so χ_{2500} is defined along the entire section. In addition, the transport above and relative to 2500 m is a large and nearly constant fraction of the total baroclinic transport across the SR3 section (Table 1) and there is little flow inshore of the 2500 m isobath on SR3 (mean ± standard deviation of 0.1 ± 2.0 Sv and 3.3 ± 2.0 SV at the northern and southern ends, respectively).

[20] Using data from the six occupations of SR3, we found that a tight relationship exists between $\overline{T}_{650}$, temperature averaged between 600 and 700 m depth, and χ_{2500} (Figure 4). Despite the fact that the cruises were made in different seasons and in different years, the scatter of the points is small. Two smoothing splines are fit to the observations. The curve covering the complete temperature range applies to all casts south of the Subtropical Front. North of the Subtropical Front, the water masses have a different $T - S$ structure, resulting in a different relationship between χ and $\overline{T}_{650}$. The location of the STF, defined by temperatures at 150 m depth greater than 11°C [*Rintoul and Bullister*, 1999], is easy to determine from temperature observations alone, and so shifting from one curve to the other when crossing the front is straightforward. The curves fit to the data in Figure 4 can be used to determine χ at each XBT cast, and hence the baroclinic transport between any pair of stations.

3.3.1. Testing the χ - $\overline{T}_{650}$ Relationship

[21] To test the accuracy of this method of inferring transport from XBT temperatures, we withheld each of

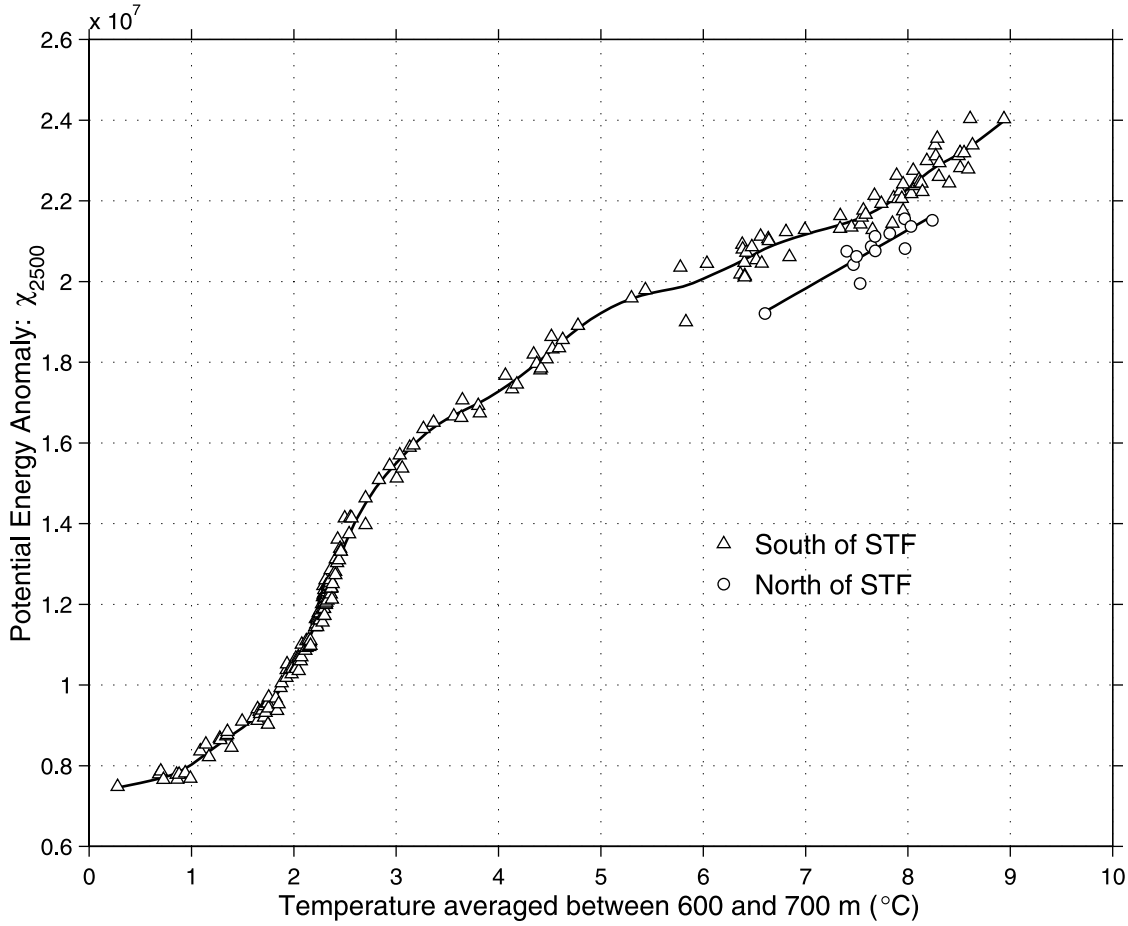

Figure 4. Potential energy anomaly integrated between 2500 dbar and the sea surface (χ_{2500}) versus temperature averaged between 600 and 700 m depth ($\overline{T}_{650}$). Data comes from all six occupations of the SR3 section. The curve is a smoothing-spline fit to the data. A separate curve is fit to stations north of the Subtropical Front (STF) (circles).

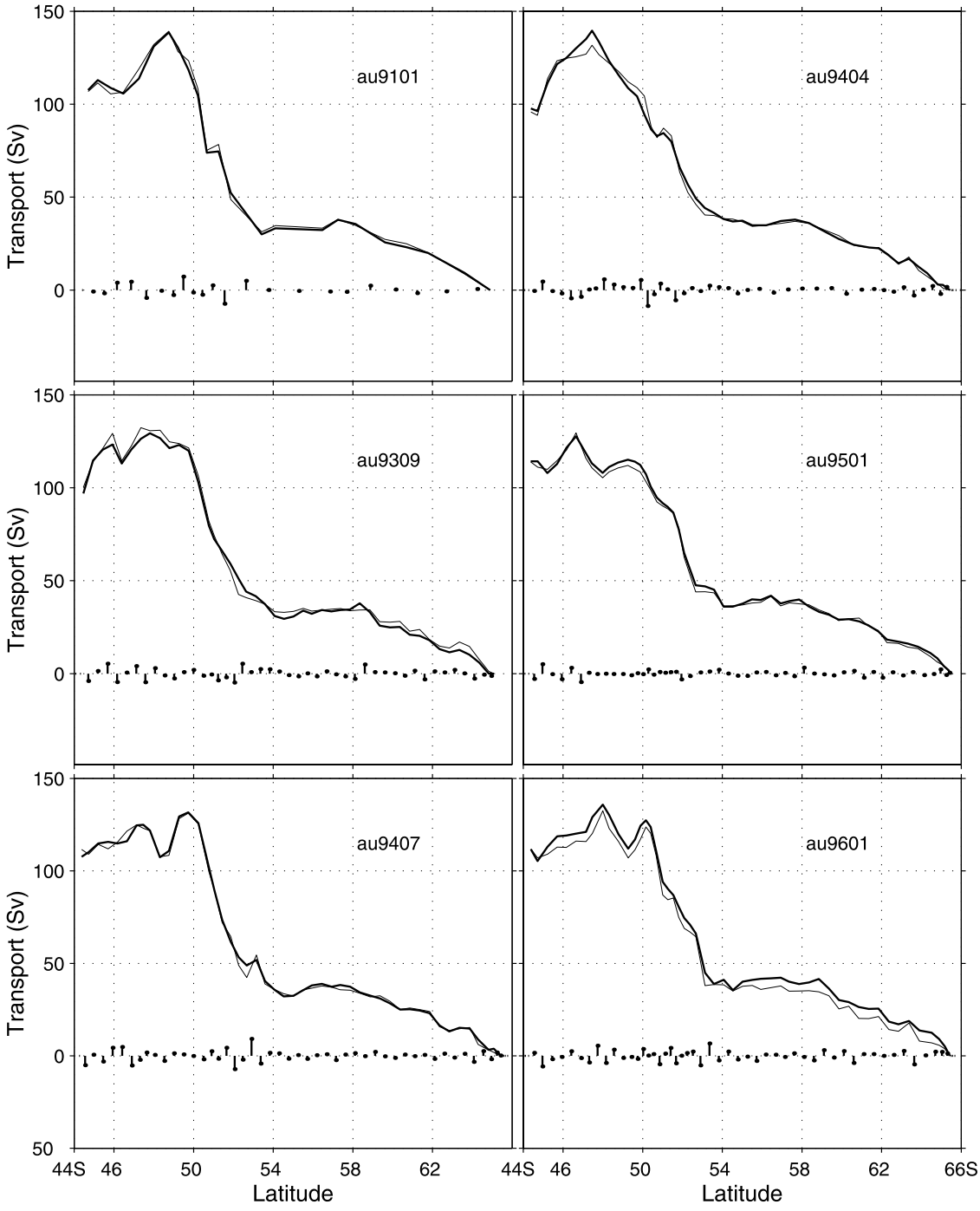

Figure 5. Comparison of cumulative transport (integrated from south to north) above 2500 dbar derived from the empirical relationship between χ_{2500} and temperature in Figure 4 (thin line) and transports calculated from the full CTD data (bold line). The comparison is made for each of the six repeats of SR3 (data from the relevant section are withheld from the empirical fit for each of these comparisons). Differences in transport at each station pair are shown by the bars along the x axis.

the six CTD sections in turn from the χ - $\overline{T}_{650}$ fit, and predicted χ using temperature observations from the withheld CTD section. The results are shown in Figure 5.

[22] The agreement between the two estimates of transport is excellent. The RMS error in station pair transports ranges from 1.7 to 3.2 Sv for the six sections, with a mean RMS of 2.6 Sv, or 2.5% of the mean transport above and relative to 2500 m. In particular, each of the main transport features (i.e. fronts) is well captured by the temperature-based transport estimate. The errors are larger near the SAF, where the transports themselves are larger, but otherwise vary randomly with latitude, with no sign of a systematic bias. The maximum error in the net transport across each section is 4.0 Sv, comparable to that in individual station

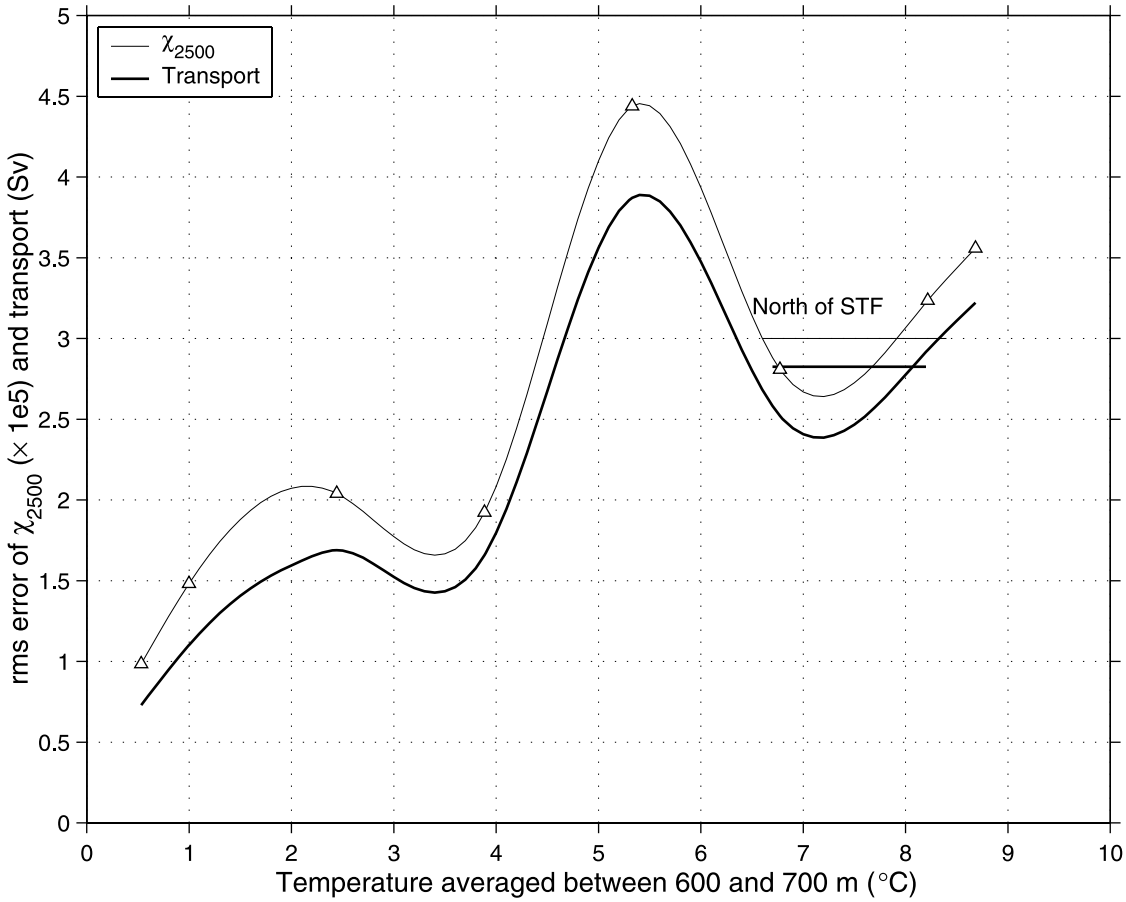

Figure 6. Distribution of RMS error in χ_{2500} and volume transport (above and relative to 2500 m, in Sv) as a function of $\overline{T}_{650}$. The error in χ_{2500} is estimated from the scatter about the smoothing spline fit in Figure 4, evaluated separately in 7 bins of $\overline{T}_{650}$ as indicated by the triangles. These errors in χ_{2500} result in the transport errors indicated by the bold line (where transport has been evaluated from differences in χ_{2500} over a one degree change in latitude). Error bars for stations north of the STF are indicated by the short line segments between 6.8° and 8.2°C.

pairs, as expected from the geostrophic relationship (the geostrophic transport across a section depends only on the end points, provided there is no intervening bathymetry and ignoring changes in the Coriolis parameter). The maximum error in net transport is slightly higher than for individual station pairs because the scatter of points in the $\chi - T$ relationship is larger at the northern (warm) end of the section (Figure 4), resulting in larger χ and transport errors (Figure 6).

[23] Another source of error in the net transport from XBT data results from extrapolation of incomplete XBT sections. Of the total of 45 sections, 19 sections reached to the middle of the continental slope (depths of 1900 to 2500 m) at both ends of the section. Another 12 sections were complete at the northern end, but did not reach the Antarctic continental slope (mainly due to weather and sea ice conditions). However, the transport variability at the southern end of the section is small (standard deviations less than 2.5 Sv south of 62°S, Figure 7), and the error associated with the $\chi - \overline{T}_{650}$ relationship is also small there (Figure 6). We can therefore extrapolate those sections with gaps at the southern end without introducing large uncertainties, and these 12 sections were also used. The error bars for the net transport estimates discussed in the following sections include both the method error (Figure 6) and, where applicable, the extrapolation error. Extrapolation at the northern end is not possible due to the larger transport variability and larger method errors there, so the 14 sections with incomplete northern ends were not used.

3.3.2. Mean Transport Versus Latitude

[24] The meridional distribution of mean baroclinic transport across the SR3 and SURVOSTRAL sections is shown in Figure 7. The transport distribution is similar at both sections: westward flow at the northern end of the section; a broad peak of strong eastward flow between 49° and 55°S; a band of weak flow south of 55°S; and three transport maxima south of 58°S. The main peak includes the SAF, the northern branch of the PF, and the eastward limb of an anticyclonic recirculation in the SAZ [*Rintoul and Sokolov*, 2001]. The three prominent maxima south of 55°S correspond to the southern branch of the PF, the southern ACC front, and the southern boundary of the ACC. The frequent presence of a meander or ring north of the SAF, with westward flow near 49°S, shows up in the mean as a transport minimum at both sections. The band of weak, alternating flow south of the SAF is

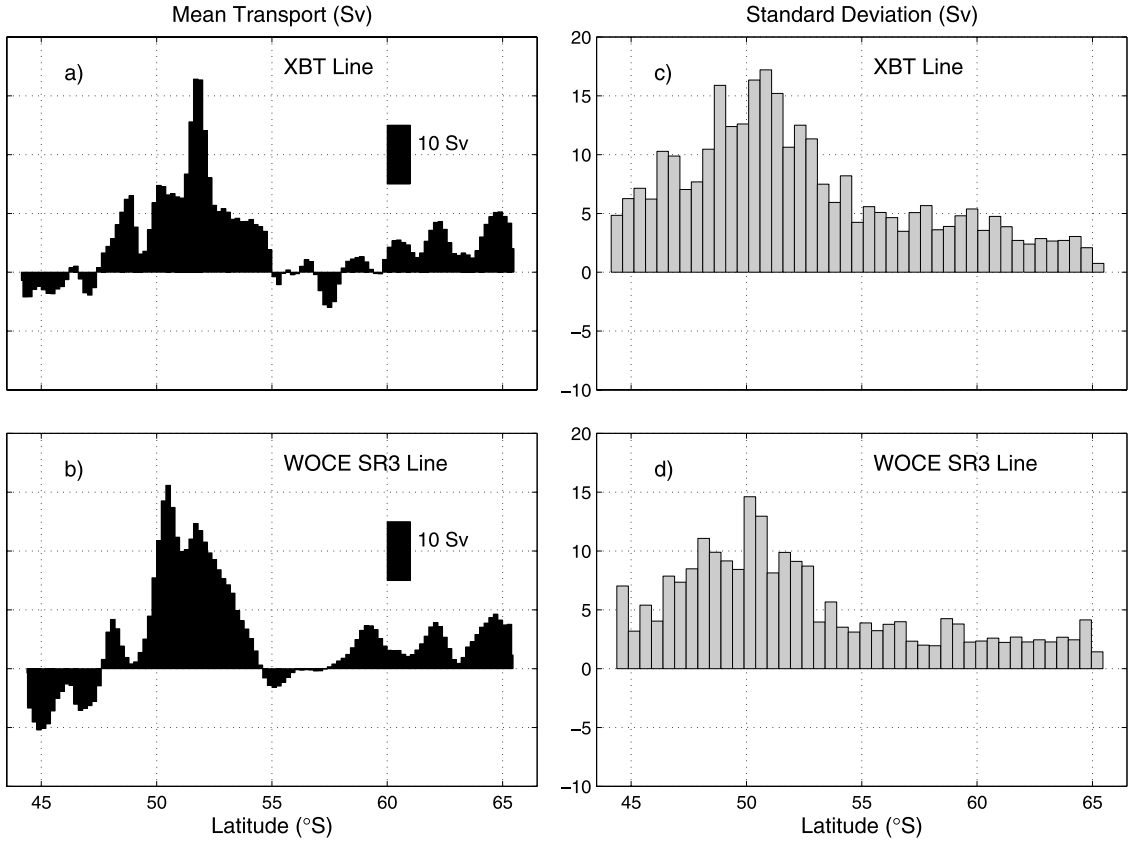

Figure 7. Mean volume transport per unit width (so area under the curve is equal to transport, area of scale bar = 10 Sv) along the (a) SURVOSTRAL XBT line and (b) WOCE SR3 line. The standard deviation of cumulative transport integrated from south to north along the (c) XBT line and (d) SR3 line. The XBT mean transports are estimated from 31 austral summer XBT sections. The SR3 mean transports are estimated from six repeats of SR3.

broader on the SURVOSTRAL section (55° to 60°S), consistent with the mean dynamic height pattern in Figure 1 which shows the flow is roughly along the section in this latitude band.

[25] The meridional distribution of variability in the cumulative transport is also similar at the two sections (Figure 7). The largest standard deviations are found in the SAF and the Subantarctic Zone (SAZ). Variability south of 55°S is weak (standard deviations less than 5 Sv). Note that these standard deviations in latitude bins reflect both shifts of front location and changes in current strength.

3.3.3. Time Series of Section-Integrated Baroclinic Transport

[26] A time series of austral summer transport across the 31 complete SURVOSTRAL sections between 1993 and 1999 is shown by the squares in Figure 8a. The transport is integrated along the XBT line between the 2500 m isobaths. (The other symbols in Figure 8a are derived from CTD and altimeter data and are described below). The mean transport across the XBT line (above and relative to 2500 dbar, U_{2500}) is 109 Sv, with a standard deviation of 4.9 Sv, similar to the mean transport across SR3 of 106 Sv (standard deviation of 7.2 Sv). There is no clear pattern of variation in net transport within an austral summer season in Figure 8. Rather, the section-to-section variability is dominated by shifts of up to 10 Sv on timescales of a few weeks.

[27] The mean austral summer transport inferred from XBT data increased between 1993 and 1997 by about 8 Sv, or 7%, then decreased in 1998 and 1999, as illustrated by the thick dashed line in Figure 8. Note that since χ is inferred from temperatures, an increase in net transport corresponds to an increase in the temperature difference between Australia and Antarctica. The temperature at the southern end of the section is relatively constant with time, so larger transports generally correspond to warmer temperatures (a deeper thermocline) at the northern end of the section.

3.4. Baroclinic Transport Inferred From Altimeter Data

[28] We have XBT data only between October and March. There is therefore a risk of aliasing both high frequency and low frequency (including seasonal) variability. We next explore whether the more continuous time series of sea surface height from satellite altimetry can be used to estimate baroclinic transport.

[29] First, we compare sea level anomalies derived from in situ data along SR3 to altimeter data interpolated to the time and location of the CTD sections. The two estimates of sea level anomalies show reasonable correspondence, with an RMS difference of 0.05 m (Figure 9). Somewhat larger errors occur on parts of the January 1994 (au9407) and January 1995 (au9404) sections, when only data from

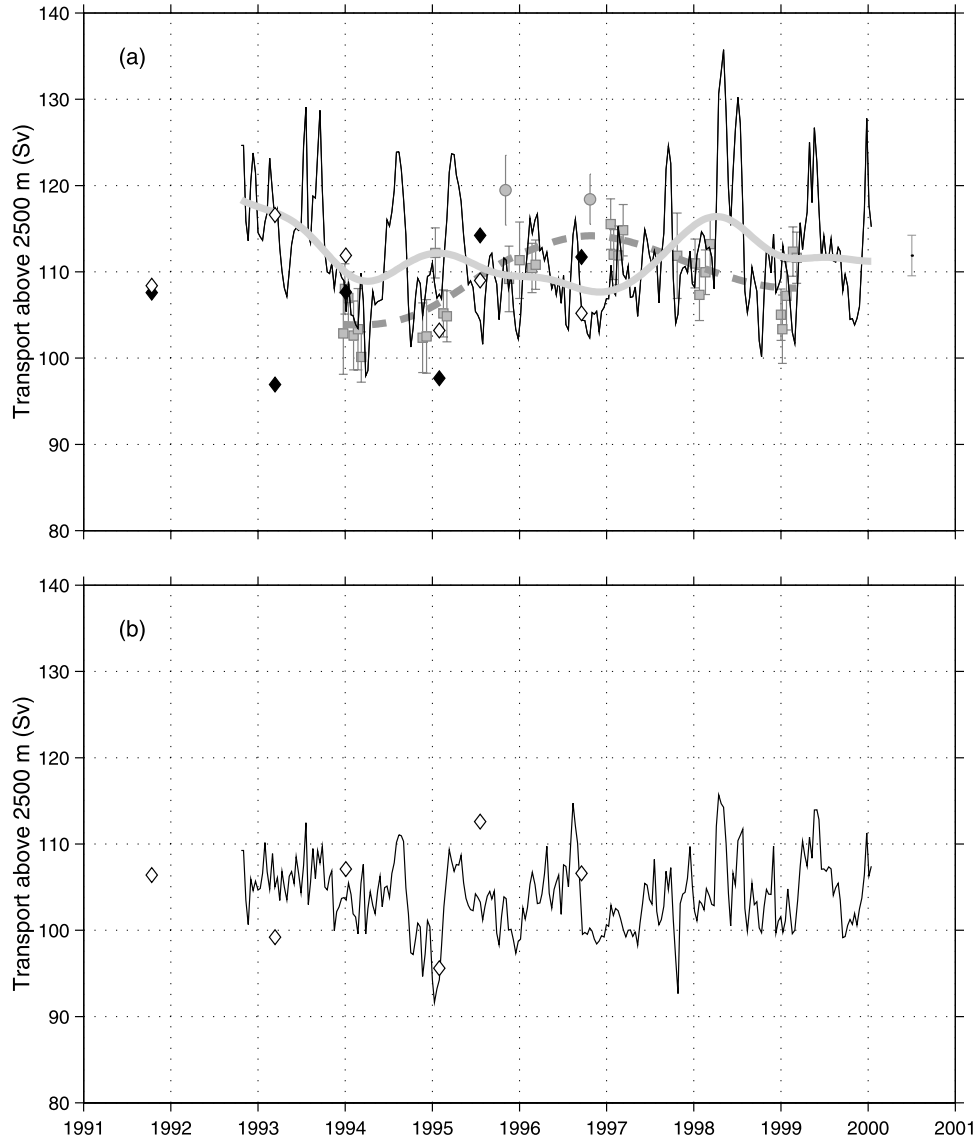

Figure 8. (a) Net baroclinic volume transport (above and relative to 2500 dbar) estimated from XBT data (squares). Two outliers (circles) are explained in the text. The apparent interannual signal inferred from a smoothing spline fit to the XBT data is shown by the thick dashed line. Net baroclinic transport derived from altimeter data is shown by the thin solid line; the low-passed interannual (periods >1.5 years) transport record is shown by the thick solid line. For comparison to the XBT data, the altimeter estimates are integrated from the south up to 45°S (see text for details). Transport above 2500 m integrated along the SR3 line to 45°S (open diamonds) and from shore to shore (filled diamonds) is also shown. Error bars are shown for each XBT estimate; the error bar on the right side shows the estimated error in the altimeter transports. (b) Net baroclnic transport above 2500 m from altimeter data, integrated from the south to 44.5°S, where the SR3 line crosses the 2500 m isobath. Transport from the SR3 CTD sections is shown by the diamonds. Tick marks on the time axis indicate the start of each calendar year.

TOPEX/Poseidon were available for the altimeter maps. Also shown in Figure 9 are sea level anomalies from each of the 10 day periods surrounding the CTD cruise, illustrating the relatively rapid variations in height near the SAF, which complicate the comparison. The signal-to-noise ratio, defined as the standard deviation of sea surface height divided by the difference between altimeter and CTD surface height estimates, is about two to three in the vicinity of the SAF (48° to 53°S), and roughly one elsewhere, with lower values over the Tasmanian continental slope.

[30] The CTD estimates of surface height anomalies relative to 2500 m depth include only the signal of changes in the density field above this level. The altimeter measurements, on the other hand, reflect changes in the density field through the full ocean depth, as well as variations in the barotropic flow. More specifically, the sea surface height anomaly (corrected for atmospheric loading) η can be written [*Gill and Niiler*, 1973]:

$$\eta = \eta_{bc} + \eta_{bt} \tag{3}$$

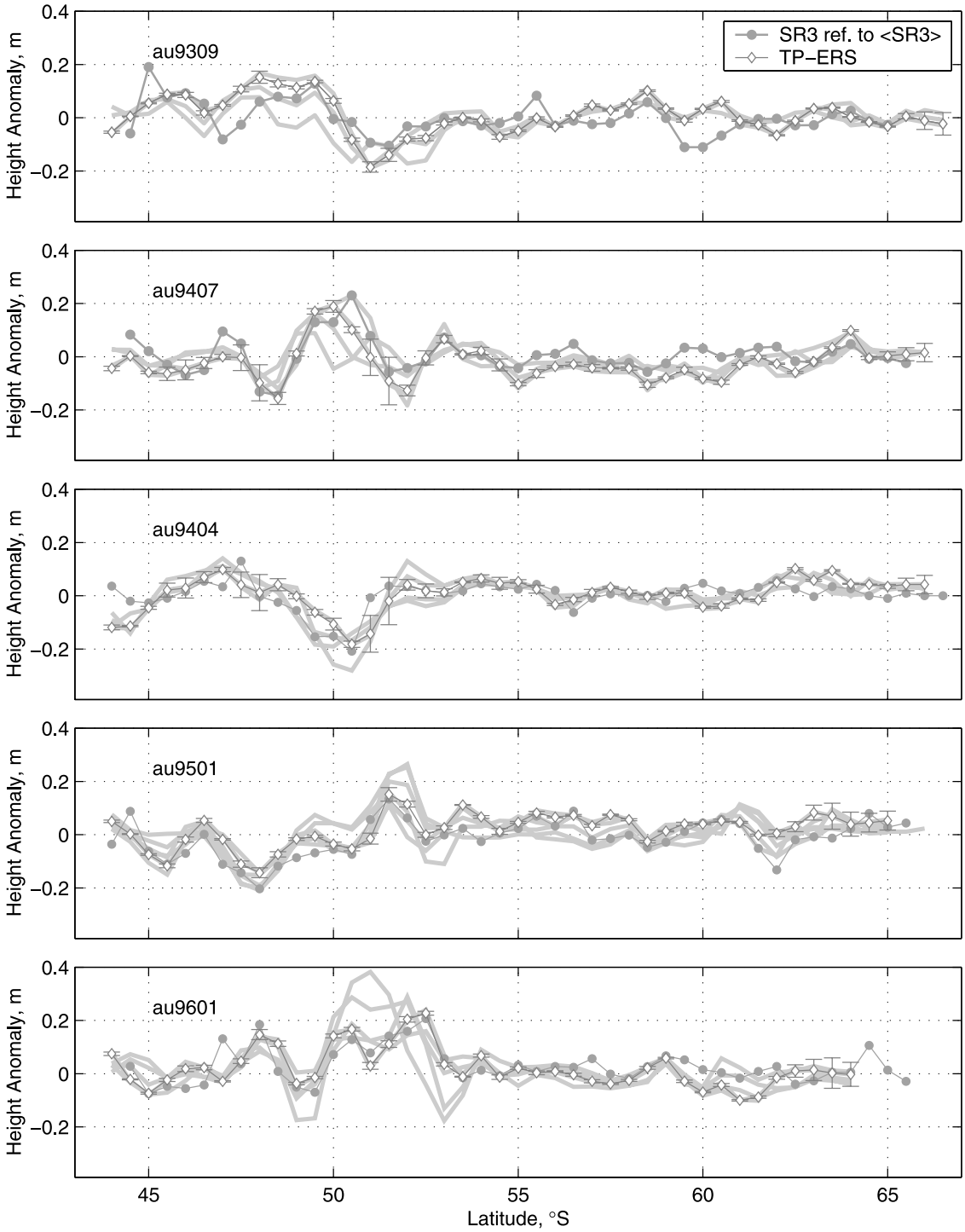

Figure 9. Comparison of SR3 surface dynamic height anomalies (dots) and sea level anomalies derived from altimeter data (diamonds) for five occupations of SR3. The dates of each cruise are given in Table 1. The altimeter data is interpolated to the space and time of the corresponding CTD station; the error bars indicate the sea surface height mapping error. Sea level anomalies from individual 10 day gridded maps coincident with the cruise, interpolated in space to the SR3 track, are shown by shaded lines. The differences between the shaded lines indicate the variability in the sea level anomaly at 10 day periods.

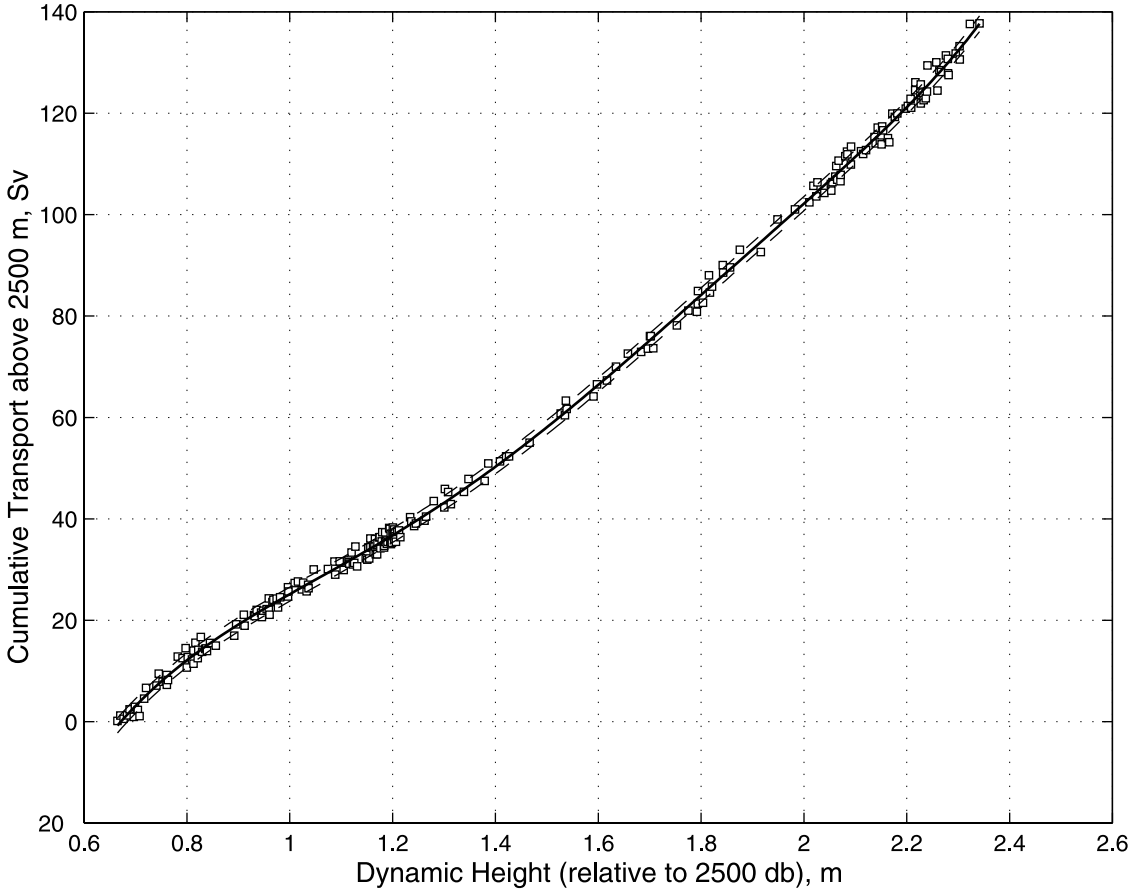

Figure 10. Cumulative volume transport (above and relative to 2500 m) integrated from the 2500 m isobath crossing at the southern end of the section versus dynamic height at the sea surface relative to 2500 m, from the six occupations of SR3.

where the baroclinic contribution

$$\eta_{bc} = \frac{1}{\rho_o}\int_{-H}^{0} \rho'(z)dz \tag{4}$$

can be divided into the contribution from the density field above and below 2500 m depth:

$$\eta_{bc}^{upper} = \frac{1}{\rho_o}\int_{-2500}^{0} \rho'(z)dz, \quad \eta_{bc}^{lower} = \frac{1}{\rho_o}\int_{-H}^{-2500} \rho'(z)dz. \tag{5}$$

The contribution of barotropic fluctuations to the sea surface height anomaly is given by:

$$\eta_{bt} = \frac{1}{g\rho_o}P_b. \tag{6}$$

In the above, η is the sea surface height anomaly, $H(\mathbf{x})$ is the water depth, ρ' is the density anomaly relative to a constant reference density ρ_0, and P_b is the bottom pressure anomaly.

[31] The differences between the CTD and altimeter curves in Figure 9 therefore in part reflect η_{bc}^{lower} and η_{bt}. The differences also reflect a number of other factors (e.g., differences in temporal and spatial sampling, mapping errors, and tides which have not been entirely removed from the altimeter signal). Despite these factors, estimates of sea surface height anomaly inferred from CTD and altimeter measurements are similar, suggesting that the altimeter signal largely reflects baroclinic changes in the upper 2500 m of the water column. In the following section, we test this idea by comparing CTD and altimeter estimates of baroclinic transport.

3.4.1. Deriving Baroclinic Transport From Altimeter Data

[32] We use the SR3 CTD data to derive an empirical relationship between surface dynamic height relative to 2500 dbar and cumulative transport, integrated northward from the 2500 dbar isobath at the southern end of SR3 (Figure 10). The relationship is very tight, suggesting we can estimate baroclinic transport from surface dynamic height. If we further assume that altimeter surface height anomalies primarily reflect changes in dynamic height (i.e., the baroclinic field), we can use this relationship to infer transport from altimetry. (We could alternatively define a relationship between dynamic height and χ_{2500}, but the cumulative transport approach avoids the problem that the altimeter data does not extend to the southern end of the section during winter due to the presence of sea ice). To use the relationship in Figure 10, we first add to the altimeter sea level anomalies the mean surface dynamic height relative to 2500 dbar calculated from the repeats of

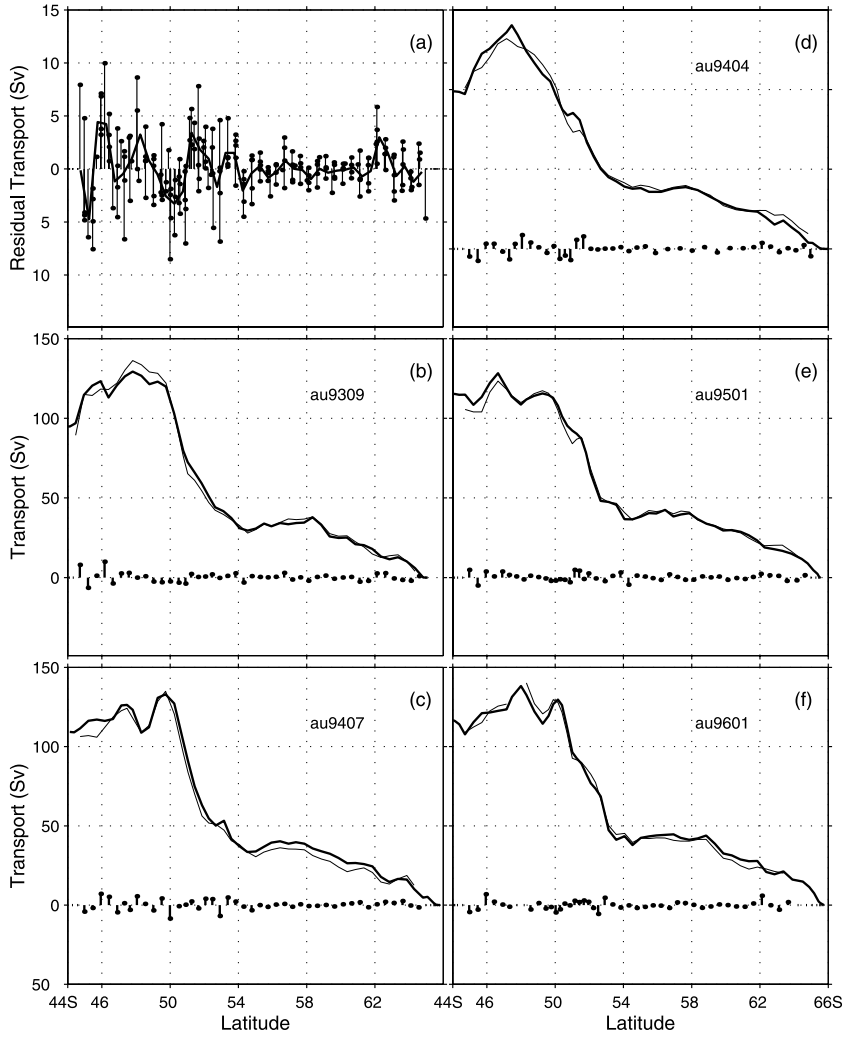

Figure 11. Comparison between baroclinic transport estimated from altimeter sea surface height (thin line) and transport from the full CTD data (thick line), for five occupations of the WOCE SR3 line, as in Figure 5. The differences between the two curves are summarized in (a); the solid line is the mean residual plotted as a function of latitude.

SR3. The mean dynamic height from the *Olbers et al.* [1992] climatology is similar to the mean of the six SR3 sections, although somewhat smoother. (The transport over the slope missed by integrating between the 2500 m isobaths is 3.3 ± 2.0 Sv (mean ± standard deviation) at the southern end and 0.1 ± 2.0 Sv at the northern end, based on six repeats of SR3.)

[33] To test this approach, Figure 11 shows a comparison between baroclinic transport estimated from altimetry and from CTD data. The structure of the cumulative transport curves is well reproduced. The station pair by station pair differences are generally less than 2.5 Sv south of 54°S, and less than 5 Sv north of 54°S, with the largest residuals less than 10 Sv. The RMS difference in net transport is 4 Sv.

[34] The small residuals support the assumption that variations in sea level primarily reflect changes in baroclinic flow above 2500 m. The residuals are not entirely randomly distributed in latitude (Figure 11a). The altimeter estimate is smaller than the CTD estimate at the southern ACC front near 62°S, between 51° and 54°S on the southern flank of the SAF and in the PF, and near 46°S. The altimeter estimate is larger between 49° and 51°S, in the core of the SAF, and near 45°S. The larger residuals near the fronts at least in part reflect the deep (>2500 m) structure of the fronts, which extend to the sea floor (e.g., Figure 2) and carry significant transport (Table 1). Mapping errors may also contribute; for example, notice that the relatively large mismatch between the altimeter and CTD curves near 47.5°S and 51°S during the January 1995 cruise (au9404, Figure 11d) corresponds with large mapping errors in the altimeter data (as indicated by the error bars on the altimeter anomaly curve in Figure 9; the mapping errors are larger during this period because only data from the TOPEX/Poseidon altimeter were available). The differences between the two curves also reflect barotropic signals in the altimeter data. If other factors (e.g., deep baroclinic flow, mapping errors and tides) contributing to the residuals are ignored, the transport residuals in Figure 11a can be translated to height residuals using Figure 10, and barotropic transport

estimated on the assumption that the height residuals reflect barotropic flow. When interpreted in this way, the residuals in Figure 11a correspond to barotropic transports which are roughly three times larger (i.e. the scale on the transport axis in Figure 11a should be multiplied by three, so the largest residuals would correspond to barotropic transports of about 30 Sv). As noted above, this is probably an overestimate of the barotropic transport because mapping errors and deep baroclinic flow also contribute to the residuals.

3.4.2. Comparison of Transport Estimated From Altimetry and XBTs

[35] We can further test the altimeter transport estimates by comparing them to the XBT time series of net transport. Because geostrophic transport estimates are sensitive to the end points, the limits of integration must be chosen carefully. The altimeter transport time series is derived from data mapped to the SR3 line, because we have an estimate of the mean dynamic height there from the repeat CTD sections. While the sections are close together at the southern end, the XBT line lies about 80 km to the east of the SR3 line at the northern end of the sections. To make a consistent comparison between estimates of transport across the two lines, we need to use comparable endpoints for the transport integration along each section.

[36] On SR3, baroclinic transport inshore of the 2500 m isobath at 44.5°S is small (0.1 ± 2 Sv), so integrating northward to the 2500 m isobath captures all the transport at the northern end. On the XBT line, we cannot estimate the transport inshore of 2500 m using the $T_{650} - \chi$ relationship because χ_{2500} is not defined there. However, the distribution of SSH variability suggests there is significant transport inshore of the 2500 m isobath on the XBT line (Figure 12). Where the two sections cross the 2500 m isobath, the SSH variability is larger on the XBT line than on SR3. Further inshore along the XBT line, the SSH variability decreases to levels similar to those observed at the inshore end of the CTD line. In other words, there are larger gradients in sea surface height (hence transport) between the 2500 m isobath and the shelf along the XBT line than along the CTD line. The SSH variability at 45°S on the CTD line is similar in magnitude and well correlated (correlation coefficient of 0.68) with the variability observed where the XBT line crosses the 2500 m isobath. The mean transport across each section south of these points is also similar. To make a consistent comparison between the two estimates, we therefore compare altimeter transport south of 45°S along the CTD line (thin solid line in Figure 8a) to XBT transport south of the 2500 m isobath crossing along the XBT line (squares in Figure 8a).

[37] The root mean square difference between simultaneous transport estimates from the XBT and altimeter data is about 4 Sv. The altimeter estimates also agree well with estimates from CTD data integrated south of 45°S (open diamonds in Figure 8a). Two XBT sections (circles) are outliers in Figure 8a. The average temperature at the northern end of the late 1995 section was higher than the temperature range covered by the $T_{650} - \chi_{2500}$ relationship, and additional uncertainty is introduced by the need to extrapolate the relationship in Figure 4. The late 1996 section had a large gap at the northern end of the section, and the transport corresponding to the 2500 m crossing was obtained by interpolation between inshore and offshore stations.

[38] The altimeter transport time series captures substantial variability which is missed by the XBT sections. As a result, the interannual transport variability inferred from the summer XBT sections (thick dashed line in Figure 8a) differs from the low-pass filtered altimeter record (thick solid line). The gradual increase in mean austral summer transport between 1994 and 1996–1997, and the subsequent decrease in the latter half of the XBT record, gives a misleading impression of the actual low-frequency transport variability. Transport variations in the mesoscale and quasi-annual band are aliased by the XBT sampling rate of six sections per austral summer.

3.4.3. A 6 Year Time Series of Net Baroclinic Transport

[39] While integrating the altimeter transport estimates to 45°S provides a time series which can be compared to the XBT time series, it does not provide the best estimate of net transport across the section because the flow between 45°S and the coast is omitted. The mean transport between 45°S and the 2500 m isobath is 9 Sv (to the west) from the six SR3 sections; the mean transport between the 2500 m isobath and the Tasmanian coast is 0.1 Sv. We can therefore estimate net transport across the SR3 line by integrating the altimeter transport northward along SR3 to the 2500 m isobath (Figure 8b). The variability is smaller in Figure 8b because transport between 44.5° and 45°S to some extent compensates transport variability south of 45°S. The mean net transport (above and relative to 2500 m, and integrated between the 2500 m isobaths) is 103 Sv, with a standard deviation of 4.3 Sv. Adding the mean transport (3 Sv) inshore of 2500 m at the southern end, and using the fact that transport above 2500 m is a nearly constant fraction of the total baroclinic transport across SR3 (Table 1), this corresponds to a top-to-bottom transport of 147 Sv ± 6.1 Sv referenced to the "best guess" level of *Rintoul and Sokolov* [2001]. (Note that the mean transports simply reflect the mean dynamic height field added to the altimeter anomalies; they are mentioned here so that the variability can be compared to the mean).

[40] To determine the dominant timescales of the transport variability, we filtered the the altimeter transport record in the mesoscale (periods <4 months), quasi-annual (4 months to 1.5 years), and interannual bands (>1.5 years). (The cutoff frequencies correspond to minima in the spectrum of sea level variability, not shown.) The standard deviation of transport is roughly comparable in each of these bands (2.3, 2.7, and 1.5 Sv, respectively). While the variability is slightly larger in the quasi-annual band, the annual signal is not very consistent from year-to-year. Figure 13a shows the amplitude of the quasi-annual signal, plotted for each year as a function of month. The timing of the maxima and minima varies, but on average the transport is about 3 or 4 Sv larger in winter than in summer. This seasonal signal contributes to the aliasing of summer-only XBT sampling.

3.5. Meridional Structure of Sea Surface Height Variability at 140°E

[41] So far we have focused on variations in the net transport south of Australia. Another important aspect of the transport variability across the SR3 and SURVOSTRAL

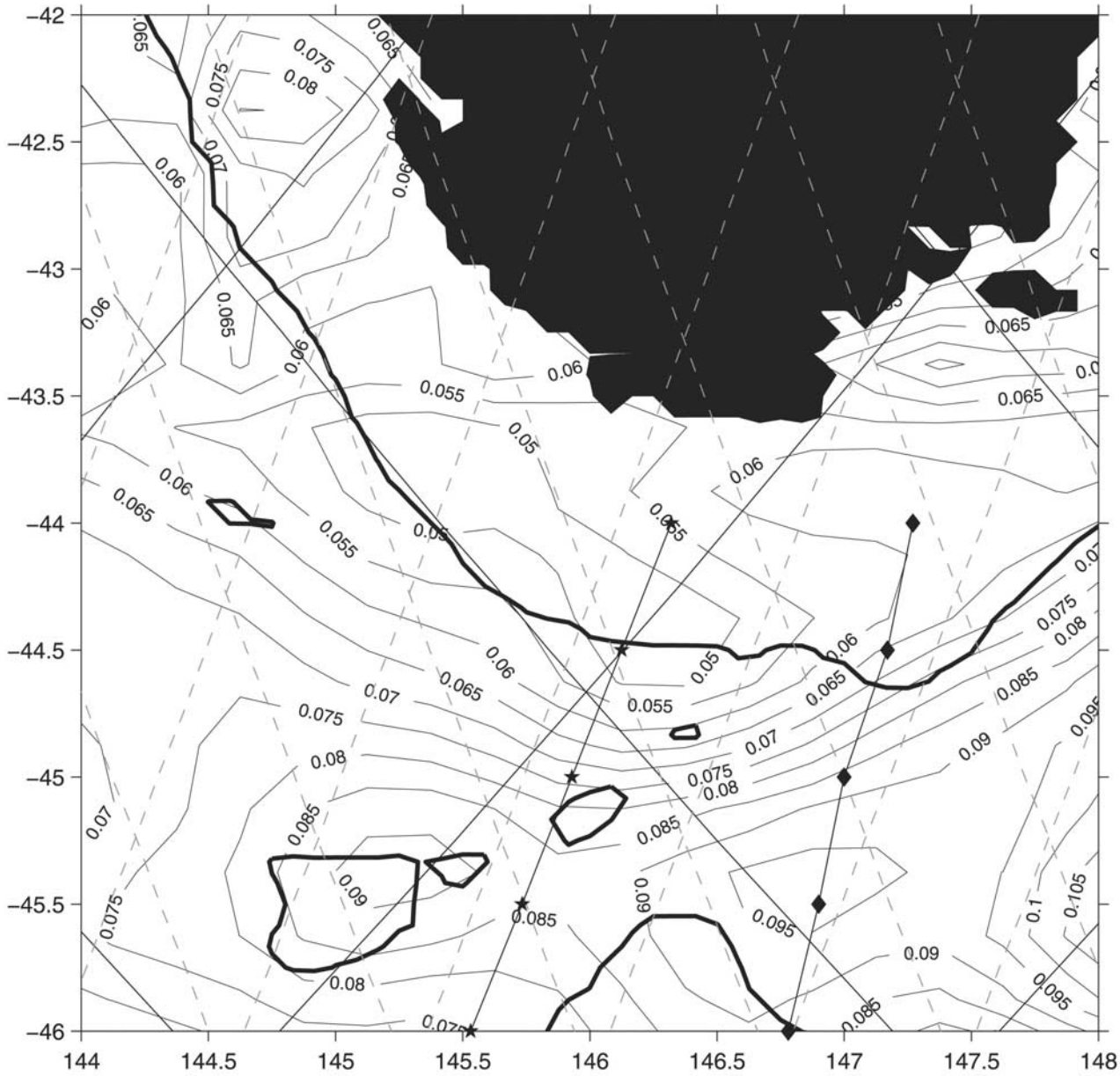

Figure 12. Standard deviation of sea surface height at the northern end of the section (contours; contour interval is 0.5 cm). The SR3 cruise track (stars) and XBT line (diamonds) are shown. The TOPEX/Poseidon and ERS satellite altimeter ground tracks are shown by thin solid and dashed lines, respectively. The bold line indicates the 2500 m isobath and the Tasmanian landmass is in black.

sections is the meridional distribution of temporal changes in sea level and volume flux. To address this question, we filtered the sea level anomaly interpolated to SR3 in the mesoscale, quasi-annual and interannual bands, using the same cutoff frequencies as above.

[42] The meridional distribution of sea level variability is similar in each band (Figure 14). Maximum variations of about 0.1 m are observed in the main jet of ACC near 50.5°S, while variability of less than 0.03 m is observed south of 53.5°S. North of the SAF, sea level variations are of moderate size (up to 0.06 m) in the quasi-annual band, and relatively small at the other frequencies. The enhanced variability in the quasi-annual band near Tasmania may reflect the seasonal extension of the East Australian Current to these latitudes [*Cresswell*, 2000].

[43] Even on a diagram presenting the smoothly varying interannual variation in sea level height at SR3 (Figure 15a), the SAF zone has a distinct three-jet structure, as also seen in the CTD section in Figure 2. The southern jet of the SAF roughly coincides with the 1.5 m sea surface height contour near 53°S. The middle branch of the SAF is found further north at 52°S (the 2.0 m contour), while the primary jet is observed at 50.5°S (2.5 m contour). The interannual variability in sea level is dominated by meridional shifts of the northern jet, with weaker interannual variability in the middle and southern branches. High variability is also

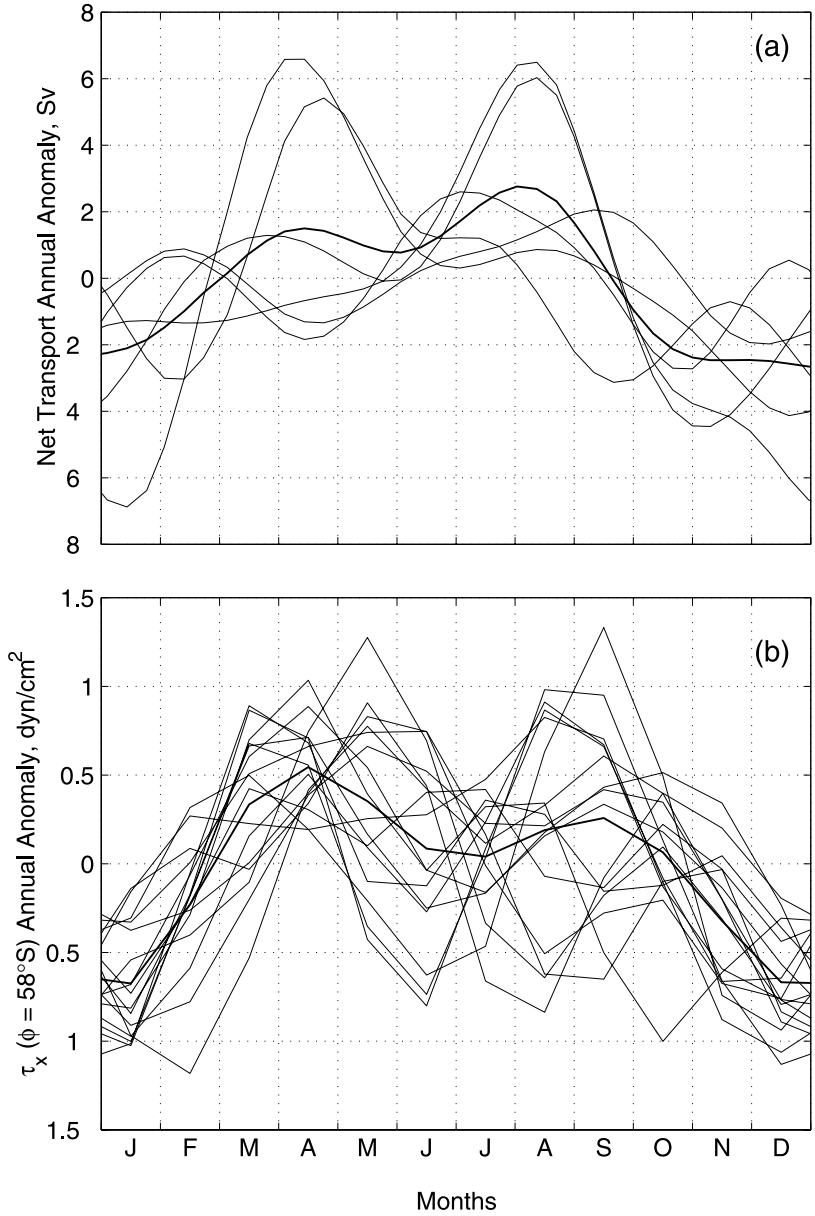

Figure 13. Variations in (a) net transport and (b) zonal wind stress at 58°S in the quasi-annual frequency band (4 months to 1.5 years). The band-passed time series is plotted in 12 month pieces (thin lines) and the mean "annual cycle" is indicated with a bold line.

apparent further north at 48–49°S and is associated with anomalous low sea levels when the cold-core eddy/meander is present.

[44] Annual variations in sea level are distributed more evenly in the SAF zone (Figure 15b). Each of the three jets meanders independently (i.e. there is no clear signal of expansion of contraction of the SAF as a whole, or a coherent meridional shift of all three cores of the SAF). Quasi-annual variability is also significant at the latitude of cold-eddy formation. Variability in this band has a secondary peak near 46°S (Figure 14), near the mean position of the STF. However, the density signal associated with the STF itself is small because the temperature and salinity gradients are largely compensating there; the height variability therefore likely reflects shifts in the boundary between the Tasman outflow and SAZ recirculation identified by *Rintoul and Sokolov* [2001], as these features extend through most of the water column and have a significant signature in surface height. Barotropic signals may also contribute.

[45] The meridional distribution of mesoscale changes in sea level across the Southern Ocean is presented in Figure 15c. Sea surface height variability in the vicinity of the SAF is about an order of magnitude larger than in the quieter regions to the north and south. North and south of the SAF the mesoscale variability has a dominant period of about 55 to 70 days and, particularly in the south, appears to be roughly in phase over a broad range of latitude. This weak, in-phase sea surface height signal may result from aliasing of tides which have not been entirely removed from the

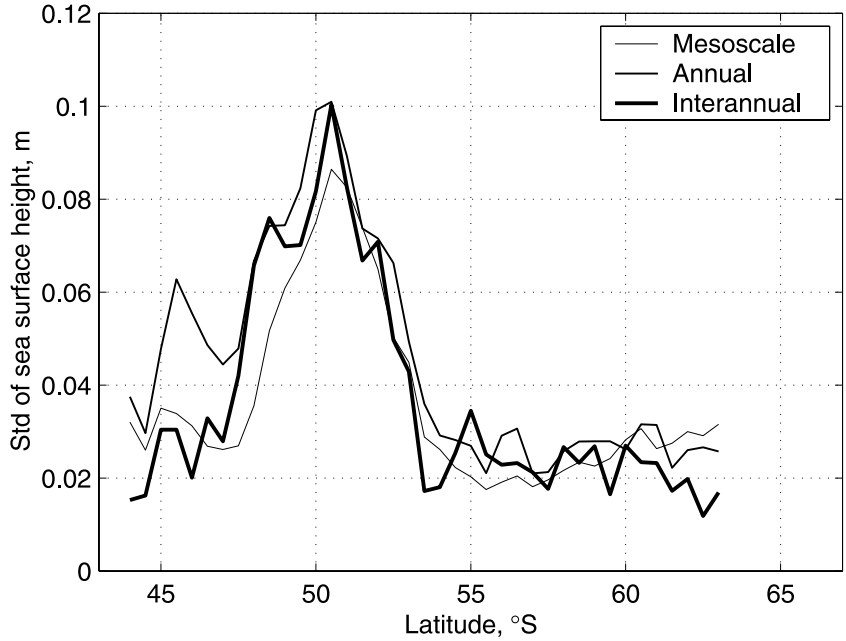

Figure 14. Meridional distribution of standard deviation of sea sea surface height in three frequency bands: interannual (periods >1.5 years), annual (4 months to 1.5 years) and mesoscale (periods <4 months).

altimeter signal (e.g., aliasing of the M_2 and S_2 tides produces a signal with a period of about 60 days) [*Shum et al.*, 1997]. Some of the net transport variability in the mesoscale band may therefore reflect an unphysical artifact in the altimeter data. However, the fact that XBT transport estimates (which are unaffected by tides) can change by 5 to 10 Sv over timescales of a few weeks suggests that physical processes contribute variance in this frequency band. Moreover, the net transport variability is largest in the quasi-annual band; in particular, the aliasing of the XBT time

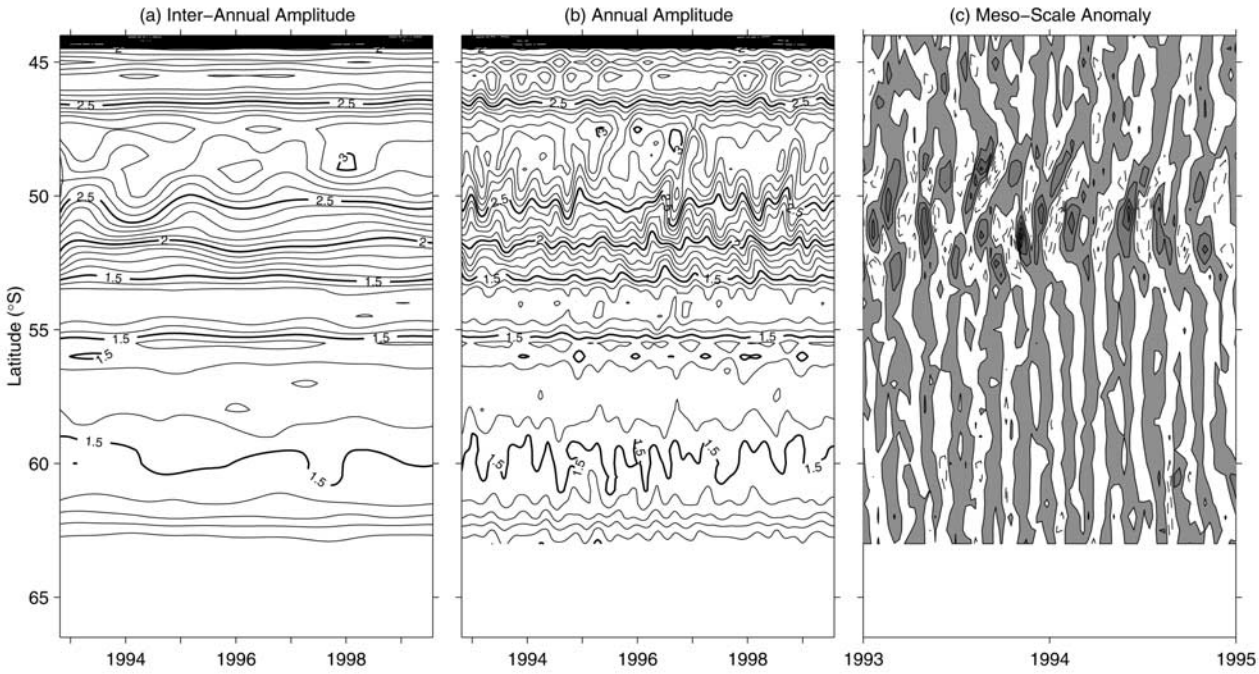

Figure 15. (a) Interannual and (b) quasi-annual variations in sea surface height (m) at SR3. (c) Sea surface height anomalies in the mesoscale band, with an expanded time axis. Positive anomalies are shaded and negative anomalies are contoured with dashed lines; the contour interval is 0.05 m.

series occurs primarily because the XBT sections miss the quasi-annual variability.

4. Connections Between Wind and Transport Variations

[46] Previous studies have sought links between ACC transport variations in Drake Passage and variations in zonal wind stress or wind stress curl [*Whitworth*, 1983; *Peterson*, 1988; *Hughes et al.*, 1999; *Gille et al.*, 2001]. These studies suggest the ACC responds to both wind stress and curl, but with no simple relationship between transport and either variable. The lack of such a relationship perhaps should be expected. The deep-reaching currents interact with bathymetry to produce bottom pressure torques which balance the curl of the wind stress [*Stevens and Ivchenko*, 1997; *Gille*, 1997; *Rintoul et al.*, 2001]; as a result, the flat-bottom Sverdrup balance, which would imply a connection between ACC transport and wind stress curl [*Stommel*, 1947; *Baker*, 1982; *Gille*, 1997; *Warren et al.*, 1996], does not apply to the ACC. Simple theoretical arguments [e.g., *Johnson and Bryden*, 1989] and linear barotropic models [e.g., *Wang and Huang*, 1995; *Krupitsky and Cane*, 1994; *Krupitsky et al.*, 1996] suggest a link between ACC transport and wind stress, but the strength of the inferred dependence on wind stress varies depending on the model assumptions [*Rintoul et al.*, 2001]. Furthermore, recent studies have also pointed out that buoyancy forcing plays a part in setting the transport of the ACC [*Gnanadesikan and Hallberg*, 2000; *Gent et al.*, 2001].

[47] Our time series of net transport, although of short duration, is still the longest record of ACC baroclinic variability yet available. Hence, we next briefly explore the relationship between transport variations and local wind stress and wind stress curl south of Australia. We use the NCEP reanalysis monthly winds [*Kalnay et al.*, 1996] interpolated to the location of the SR3 line (using zonal averages over a 40° band of longitude gives similar results). We again consider variability in the interannual, quasi-annual, and mesoscale frequency bands.

[48] In the interannual band, variations in net baroclinic transport are correlated with both wind stress and wind stress curl over a broad span of latitudes (Figure 16a). While correlations above 0.49 are significant at 95% confidence (shaded in Figure 16a), the statistics for the interannual band must be viewed with caution given the short length of the record. The strongest correlations with wind stress are found south of the core of the ACC (52° to 63°S), with wind stress changes leading transport changes by 3 to 10 months. Wind stress curl is also correlated with the net baroclinic transport (Figure 16b). The correlation changes sign at about 55°S, where the curl itself changes sign, consistent with changes in Ekman pumping driving changes in isopycnal slope and transport. At the maximum postive correlation in the Subantarctic Zone, wind stress curl changes lead changes in transport by about 8 months. However, the correlations between net transport and both wind stress and curl may reflect the fact that wind stress and curl are themselves strongly correlated, as noted by *Gille et al.* [2001]. South of Australia, we indeed find that wind stress and wind stress curl are highly correlated in all three frequency bands (not shown).

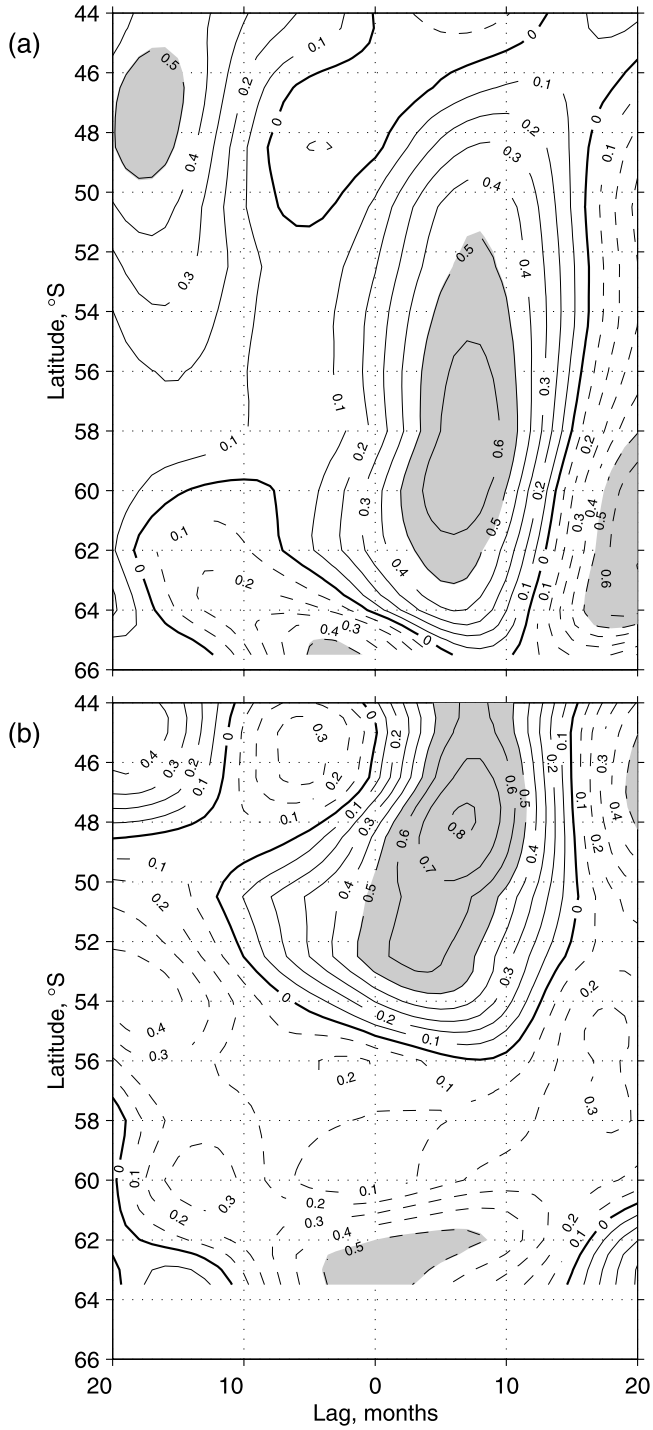

Figure 16. Lagged correlations between net transport across SR3 derived from altimeter data and (a) zonal wind stress, (b) wind stress curl along the SR3 line, for the interannual frequency band. Values above 0.49 are significant at 95% confidence (shaded).

[49] Net transport is also significantly correlated with wind stress and wind stress curl at quasi-annual times scales (not shown), although the correlations are weaker and the region of highest correlation is shifted somewhat to the south. *Gille et al.* [2001] argued, after *Chelton* [1982], that a correlation of wind forcing and ACC transport at annual

frequencies should be expected, because both would respond to the annual cycle in radiative forcing of the Earth. However, the transport variability in the quasi-annual band does not mirror the fixed annual cycle of insolation: the timing of the maxima and minima are not consistent from year-to-year (Figure 13). *Whitworth and Peterson* [1985] noted a similar feature in the Drake Passage transport time series, which they described as an annual cycle that was ''not phase locked.'' The quasi-annual variability in wind stress at 58°S (the latitude of maximum correlation between stress and transport) is dominated by the semiannual signal expected in this region, but it also is not ''phase locked'' from year to year (Figure 13b). Given that 45% of the transport variability with periods >20 days and 60% of the wind stress variability with periods >2 months is in this frequency band, the factors responsible for the irregular nature of the quasi-annual oscillations are an important area for future research. In this regard, it is interesting to note that the amplitude of the quasi-annual transport variations was large in 1993–1995 and 1998–1999 (about ±6 Sv), in comparison to 1996–1997 (less than ±3 Sv). Periods of relatively large quasi-annual variability coincide with positive interannual anomalies in eastward wind stress, perhaps indicating nonlinear ACC dynamics.

[50] A more complete discussion of links between baroclinic transport variations and wind forcing awaits a longer transport time series. Such a study should also try to isolate transport changes of the ACC itself from those of the flows north of the ACC, which *Rintoul and Sokolov* [2001] show have a substantial impact on the net transport between Australia and Antarctica.

5. Discussion

5.1. Assessment of Proxy Methods for Inferring Baroclinic Transport

[51] We have explored two proxy techniques for estimating baroclinic transport, first from subsurface temperature and second from sea surface height. Both techniques succeed in producing good transport estimates along the SR3 line, as evaluated by comparing transport estimated from the complete CTD data to estimates using the proxy methods. However, this first attempt to use proxy methods to obtain frequent, accurate transport estimates of the ACC has also revealed some of the limitations of such approaches. For example, we found that while the method used to infer transport from subsurface temperature was highly successful on the SR3 line (e.g., Figure 5), the particular cruise track of the XBT line was not optimal for obtaining good estimates of net transport using this particular method because some transport was missed inshore of the 2500 m isobath. Further experimentation is required to see if refinements to the method can capture the missed transport over the upper continental slope. While the location of the XBT line may not be ideal for estimating net transport, it is important to note that the method performs well along the entire latitude band spanned by the SR3 section (Figure 5). The repeat XBT lines can therefore reveal variations in the strength and location of the major fronts between Tasmania and Antarctica (e.g., Figure 7).

[52] A second limitation of the repeat XBT lines for transport monitoring is their temporal sampling. The altimeter-derived transport time series demonstrates that the austral summer (October to March) XBT lines miss a significant portion of the transport variability. It is therefore important to complement the ship-based programs with more continuous sampling from satellites and moorings. Nevertheless, repeat CTD and XBT sections remain an essential part of an overall Southern Ocean observing system. Full depth, coast-to-coast hydrography provides the most accurate estimates of baroclinic transport and therefore remains the ''gold standard'' against which other proxy techniques are judged. A number of other important properties can also only be measured with repeat hydrographic sections (e.g., transport changes in density classes, tracer distributions, changes in temperature and salinity in the ocean interior, and variability in the transport of heat, salt and other properties). Measurements of upper ocean temperature from frequently repeated XBT sections similarly provide information on the vertical distribution of changes in thermal structure which cannot be obtained in any other way.

[53] Some earlier attempts have been made to use altimetry to infer ACC current speeds or transports. Most often, geostrophic surface currents are inferred from height differences [e.g., *Challenor et al.*, 1996; *Gille et al.*, 2001]. However, some information on the distribution of velocity with depth is required to translate the surface velocity estimates into transports. *Stammer et al.* [1996] assumed a linear velocity profile in a wedge-shaped channel to infer transports in Drake Passage. The advantage of the approach presented here is that ACC transports are inferred from sea surface height in a manner which accounts for the observed baroclinic structure of the ACC.

[54] All geostrophic transport estimates, whether from CTD data, XBTs or altimetry, are sensitive to the treatment of the endpoints. Near the coast, a number of factors contribute to make the use of altimeter data for transport estimates particularly challenging. The tide models used to remove the tidal signal from altimeter data are less successful over the continental shelves [*Shum et al.*, 1997]. Mapping the altimeter data is also more difficult near the coasts, so that current variability may be underestimated near the shelf break and upper slope [*Ducet et al.*, 2000]. For applications where continuous, highly accurate measurements of net transport are required, moorings will be needed. A single mooring at each endpoint, however, is unlikely to be sufficient because it is necessary to capture the flow over the continental slope, as described above. Moreover, we are ultimately interested in more than just net volume transport. To estimate heat and freshwater transport, measurements of velocity, temperature and salinity are required along the section. This cannot be done from endpoint monitoring alone.

5.2. Comparison to Previous Measurements South of Australia

[55] The distribution of transport with latitude inferred from the 31 XBT sections is similar to that observed on the six repeats of the SR3 line. Each shows westward flow at the northern end of the section, strong eastward flow in the SAF, and three weaker cores of eastward flow further south (Figure 7). However, the time series obtained from the XBT and altimeter data provide a different perspective on the

transport variability to that described by *Rintoul and Sokolov* [2001] on the basis of six occupations of the SR3 CTD section. They found substantial variability in the net transport of volume, heat, salt and other properties across the section.

[56] For example, temperature flux varied by 139°C Sv, or 0.57×10^{15} W relative to 0°C. The heat flux variability south of Australia could be balanced in a number of ways: by changes in barotropic heat transport; by local or basin-scale heat storage; by changes in zonal heat transport at the other Southern Ocean ''chokepoints''; or by air-sea fluxes. In the absence of observations of the variability in each of these terms, they could not assess the climate impact of the variations they observed at SR3.

[57] In particular, from the small number of repeats of SR3 it was impossible to determine how long the transport anomalies persisted. Figure 8 suggests that anomalies in net transport are rarely maintained for more than a few months at a time. The changes in interbasin heat exchange (the time integral of the heat flux anomalies) are therefore likely more modest than would be inferred, e.g., by assuming the anomalies observed on each SR3 section were typical of the period between the sections.

5.3. Comparison to Drake Passage

[58] Most of what we know about the transport of the ACC has been derived from measurements in Drake Passage. *Whitworth* [1983] estimated the mean transport above and relative to 2500 m to be 87 Sv, with a standard deviation of 5.5 Sv. (Transport between 500 and 2500 m was derived from one year records from dynamic height moorings on the 2500 m isobath at either end of the passage, and transport above 500 m was estimated from 20 historical hydrographic sections.) The mean baroclinic transport south of Australia (relative to the same reference level) is 103 Sv, significantly higher than at Drake Passsage [*Rintoul and Sokolov*, 2001]. The baroclinic transport variability south of Australia is somewhat smaller than that in Drake Passage (standard deviation of 4.3 Sv).

[59] In Drake Passage, estimates have also been made of the variability of the net absolute transport above 2500 m. During the International Southern Ocean Studies (ISOS) experiment, the mean net transport was estimated from hydrography, current meters and pressure gauges to be 124.7 Sv with a standard deviation of 9.9 Sv [*Whitworth and Peterson*, 1985]. During WOCE, the observed variability was somewhat smaller, with standard deviations over individual 1 year deployments ranging from 5.3 Sv in 1993 to 8.9 Sv in 1990 [*Meredith et al.*, 1996]. These estimates were derived from differences in bottom pressure across Drake Passage and rely on the assumption that the pressure records reflect variations in barotropic flow. However, evidence from ISOS and later experiments shows that while the barotropic variability may be larger and of higher frequency, the baroclinic variability cannot be ignored. For example, the linear regression model of *Whitworth and Peterson* [1985] results in transport errors with a range of 39 Sv and a standard deviation of 5.9 Sv which are very coherent with baroclinic transport between 500 and 2500 m (their Figure 6). A number of more recent studies in Drake Passage based on observations and models have similarly concluded that baroclinic variability makes a significant contribution to variations in bottom pressure and transport [e.g., *Peterson*, 1988; *Woodworth et al.*, 1996; *Meredith et al.*, 1997; *Hughes et al.*, 1999].

5.4. Baroclinic Versus Barotropic Transport Variability

[60] In this paper we have discussed only the baroclinic transport. In particular, our estimates of transport derived from altimeter data assume that η_{bc}^{upper} makes the dominant contribution to the height anomalies measured by the altimeter. The small residuals in Figure 12a are consistent with the assumption that $\eta_{bc}^{lower} + \eta_{bt}$ make a smaller contribution to η. However, these results should not be interpreted to mean that there is no barotropic flow. As noted above, even the relatively small residuals in Figure 11 would correspond to barotropic transports of 10 to 30 Sv at some station pairs, if the residual height anomalies were solely due to barotropic flow. Other studies have found evidence for significant barotropic transport in the Southern Ocean, particularly near the continental margin and in the ACC fronts [*Fahrbach et al.*, 1994; *Heywood et al.*, 1999; *Donohue et al.*, 2001; *Phillips and Rintoul*, 2002]. Barotropic currents likely also play an important role in the dynamics of the fronts (e.g., eddy mean flow interaction) and the interaction of fronts with topography. Nevertheless, the results presented here suggest the altimeter SSH anomalies largely reflect baroclinic changes in the upper 2500 m.

[61] The dominance of the baroclinic signal in the height anomalies may at first seem surprising at these latitudes. Simple theory [e.g., *Gill and Niiler*, 1973] suggests that the barotropic term will dominate at high latitudes. Some authors have therefore assumed that the sea surface height field provides a stream function for the barotropic transport ($\psi = \frac{gH}{f}\eta$). However, *Stammer* [1997] demonstrates that this is a poor assumption (outside of perhaps the North Pacific), and that the baroclinic contribution to the sea surface height cannot be ignored. *Stammer et al.* [1996] show that in the 1/4° global Parallel Ocean Climate Model (POCM) the baroclinic field below 200 m depth explains a larger fraction of the SSH variance along the axis of the ACC than do either the barotropic or shallow baroclinic contributions (between 60 and 80% of the variance in some locations, and between 40% and 60% elsewhere). In the model, barotropic fluctuations are important in the higher latitudes of the Southern Ocean, south of the ACC. (Note that the high frequency barotropic signals in some regions of the Southern Ocean discussed by *Stammer et al.* [2000] are small in amplitude near the SR3 section and unlikely to complicate the SSH signals analyzed here.)

[62] Ultimately, we are interested in the absolute transport of the ACC and need to monitor both the baroclinic and barotropic flow. However, the long-term, highly accurate, in situ measurements of absolute velocity required to directly estimate transport across long sections are difficult to make with present techonology. Determining the contribution of the barotropic flow to Southern Ocean transports therefore remains a challenging but important task. Progress is likely to be made through a combination of approaches, including: high precision altimetry (particularly combined with a time-varying gravity mission); repeat sections; moored measurements in key locations; improvements in accuracy and coverage of acoustic Doppler current profiler measurements; floats and drifters; and diagnostic models capable

of synthesizing these diverse observations with dynamical constraints.

6. Summary and Conclusions

[63] Our knowledge of the variability of the ACC and interbasin exchange is poor because of the lack of observations in the Southern Ocean. Repeat and one-time hydrographic sections obtained during WOCE have helped fill some of the gaps, but the sampling is still sparse. One aim of this paper is to explore whether alternative techniques, in particular XBT sections and altimetry, can be used to make frequent, accurate estimates of baroclinic transport with high spatial resolution.

[64] We have shown that the tight correlation between upper ocean temperature and the baroclinic transport stream function can be exploited to derive estimates of transport above and relative to 2500 dbar from temperature measurements with an error of a few per cent. The mean distribution of transport with latitude is similar at the CTD and XBT lines: westward flow at the northern end of the section; a broad band of strong eastward flow associated with the SAF and NPF; weak alternating flow between the NPF and SPF; and three persistent cores of eastward flow south of 59°S. Variability is greatest near the SAF, is weak south of 55°S, and of intermediate strength in the Subantarctic Zone.

[65] A similar relationship between surface dynamic height and cumulative transport can be used to estimate baroclinic transport from altimeter data, under the assumption that SSH anomalies measured by the altimeter largely reflect baroclinic changes above 2500 m. A comparison of transport estimated from CTD data and from altimeter data supports this assumption, although barotropic signals likely also contribute. The ten day sampling period of the altimeter transport record shows that the austral summer XBT sections alias variability at unresolved timescales.

[66] The 6 year baroclinic transport time series derived from altimeter data provides the first record of sufficient continuity and duration to infer the timescales of ACC variability. The mean net transport across SR3 is 103 Sv (above and relative to 2500 m) with a standard deviation of 4.3 Sv. Using the fact that transport above and relative to 2500 m is observed to be a nearly constant fraction of the top-to-bottom transport at SR3 (Table 1), this corresponds to a transport of 147 ± 6.1 Sv in total baroclinic transport. Transport variability in the mesoscale (periods <4 months), quasi-annual (4 months to 1.5 years), and interannual (>1.5 years) bands is 2.3, 2.7 and 1.5 Sv, respectively. While the quasi-annual band makes the largest contribution to the transport variability, the timing of extrema in the amplitude of the quasi-annual signal varies from year-to-year. On average, the net baroclinic transport is slightly higher (3 to 4 Sv) in winter than in summer. Some of the variability in the mesoscale band may reflect aliased tidal signals which have not been completely removed from the altimeter data.

[67] The proxy techniques explored here are sufficiently promising to justify further effort to refine them further. Repeat sections should be used to examine the applicability of these techniques to other locations in the Southern Ocean (and perhaps other basins). By exploiting correlations between other properties of interest, such as (transport-weighted) temperature and salinity, it may be possible to infer heat and salt as well as volume fluxes. It is also important to explore where the methods fail, and why. Such studies will help define the combination of instruments and techniques required for effective monitoring of the Southern Ocean.

[68] **Acknowledgments.** We thank Rick Bailey, Peter Jackson and Ann Gronell of CSIRO, Rosemary Morrow of LEGOS (France) and Dean Roemmich (Scripps, USA) for their help with the XBT program. Neil White provided access to the satellite altimeter data. We also thank the captains, officers, crew, scientists and volunteer observers on *Aurora Australis* and *Astrolabe* for their help in collecting the observations. The work presented here is supported in part by ANARE (Australia), IFRTP (France), NOAA (USA), and by Environment Australia through the National Greenhouse Research Program. The altimeter products were produced by the CLS Space Oceanography Division as part of the European Union's Environment and Climate project AGORA (ENV4-CT9560113) and DUACS (ENV4-CT96-0357) with financial support from the Center for Earth Observation and the Midi-Pyrenees regional council. The ERS products were generated as part of the proposal A02.F105 by the European Space Agency.

References

Baker, D. J., A note on Sverdrup balance in the Southern Ocean, *J. Mar. Res.*, *40*, suppl., 21–26, 1982.

Botnikov, V. N., Geographical position of the Antarctic convergence zone in the Pacific Ocean, *Sov. Antarct. Exped. Inf. Bull., Engl. Transl.*, *4*, 324–327, 1963.

Challenor, P. G., J. F. Read, R. T. Pollard, and R. T. Tokmakian, Measuring surface currents in Drake Passage from altimetry and hydrography, *J. Phys. Oceanogr.*, *26*, 2748–2759, 1996.

Chelton, D. B., Statistical reliability and the seasonal cycle: Comments on "Bottom pressure measurements across the Antarctic Circumpolar Current and their relation to wind", *Deep Sea Res., Part A*, *29*, 1381–1388, 1982.

Cresswell, G. R., Currents of the continental shelf and upper slope of Tasmania, *Pap. Proc. R. Soc. Tasmania*, *133*, 21–30, 2000.

Donohue, K. A., E. Firing, and S. Chen, Absolute geostrophic velocity within the Subantarctic Front in the Pacific Ocean, *J. Geophys. Res.*, *106*, 19,869–19,882, 2001.

Ducet, N., P. Y. Le Traon, and G. Reverdin, Global high-resolution mapping of ocean circulation from TOPEX/Poseidon and ERS-1 and -2, *J. Geophys. Res.*, *105*, 19,477–19,498, 2000.

Fahrbach, E., G. Rohardt, M. Schroder, and V. Strass, Transport and structure of the Weddell Gyre, *Ann. Geophys.*, *12*, 840–855, 1994.

Gent, P., W. G. Large, and F. O. Bryan, What sets the mean transport through Drake Passage?, *J. Geophys. Res.*, *106*, 2693–2712, 2001.

Gill, A. E., and P. P. Niiler, The theory of the seasonal variability in the ocean, *Deep Sea Res. Oceanogr. Abstr.*, *20*, 141–178, 1973.

Gille, S. T., The southern ocean momentum balance: Evidence for topographic effects from numerical model output and altimeter data, *J. Phys. Oceanogr.*, *27*, 2219–2232, 1997.

Gille, S. T., D. P. Stevens, R. T. Tokmakian, and K. J. Heywood, Antarctic Circumpolar Current response to zonally averaged winds, *J. Geophys. Res.*, *106*, 2743–2759, 2001.

Gnanadesikan, A., and R. W. Hallberg, On the relationship of the circumpolar current to Southern Hemisphere winds, *J. Phys. Oceanogr.*, *30*, 2013–2034, 2000.

Heywood, K. J., M. D. Sparrow, J. Brown, and R. R. Dickson, Frontal structure and Antarctic Bottom Water flow through the Princess Elizabeth Trough, Antarctica, *Deep Sea Res., Part I*, *46*, 1181–1200, 1999.

Hughes, C. W., M. Meredith, and K. Heywood, Wind driven transport fluctuations through Drake Passage: A southern mode, *J. Phys. Oceanogr.*, *29*, 1971–1992, 1999.

Johnson, G. C., and H. L. Bryden, On the size of the Antarctic Circumpolar Current, *Deep Sea Res., Part A*, *36*, 39–53, 1989.

Kalnay, E., et al., The NCEP/NCAR 40-year reanalysis project, *Bull. Am. Meteorol. Soc.*, *77*, 437–471, 1996.

Krupitsky, A., and M. Cane, On topographic pressure drag in a zonal channel, *J. Mar. Res.*, *52*, 1–23, 1994.

Krupitsky, A., V. Kamekovich, N. Naik, and M. Cane, A linear equivalent barotropic model of the Antarctic Circumpolar Current with realistic coastline and bottom topography, *J. Phys. Oceanogr.*, *26*, 1803–1824, 1996.

Le Traon, P., F. Nadal, and N. Ducet, An improved mapping method of multisatellite altimeter data, *J. Atmos. Oceanic Technol.*, *15*, 522–534, 1998.

Meredith, M. P., J. M. Vassie, K. J. Heywood, and R. Spencer, On the temporal variability of the transport through Drake Passage, *J. Geophys. Res.*, *101*, 22,485–22,494, 1996.

Meredith, M. P., J. M. Vassie, R. Spencer, and K. J. Heywood, The processing and application of inverted echo sounder data from Drake Passage, *J. Atmos. Oceanic Technol.*, *14*, 871–882, 1997.

Olbers, D., V. Gouretski, G. Seiß, and J. Schröter, *Hydrographic Atlas of the Southern Ocean*, 82 pp., Alfred Wegener Inst. for Polar and Mar. Res., Bremerhaven, Germany, 1992.

Orsi, A. H., T. W. Whitworth III, and W. D. Nowlin Jr., On the meridional extent and fronts of the Antarctic Circumpolar Current, *Deep Sea Res.*, *Part I*, *42*, 641–673, 1995.

Peterson, R. G., On the transport of the Antarctic Circumpolar Current through Drake Passage and its relation to wind, *J. Geophys. Res.*, *93*, 13,993–14,004, 1988.

Phillips, H. E., and S. R. Rintoul, A mean synoptic view of the Subantarctic Front south of Australia, *J. Phys. Oceanogr.*, *32*, 1553–1563, 2002.

Rintoul, S. R., and J. L. Bullister, A late winter hydrographic section from Tasmania to Antarctica, *Deep Sea Res., Part I*, *46*, 1417–1454, 1999.

Rintoul, S. R., and S. Sokolov, Baroclinic transport variability of the Antarctic Circumpolar Current south of Australia (WOCE repeat section SR3), *J. Geophys. Res.*, *106*, 2795–2814, 2001.

Rintoul, S. R., J.-R. Donguy, and D. H. Roemmich, Seasonal evolution of upper ocean thermal structure between Tasmania and Antarctica, *Deep Sea Res., Part I*, *44*, 1185–1202, 1997.

Rintoul, S. R., C. Hughes, and D. Olbers, The Antarctic circumpolar system, in *Ocean Circulation and Climate: Observing and Modelling the Global Ocean*, edited by G. Siedler, J. Church, and J. Gould, pp. 271–302, Academic, San Diego, Calif., 2001.

Rosenberg, M., R. Eriksen, and S. Rintoul, *Aurora Australis* marine science cruise AU9309/AU9391: Oceanographic field measurements and analysis, *Res. Rep. 2*, 103 pp., Antarct. Coop. Res. Cent., Hobart, Tasmania, Australia, 1995a.

Rosenberg, M., R. Eriksen, S. Bell, N. Bindoff, and S. Rintoul, *Aurora Australis* marine science cruise AU9407: Oceanographic field measurements and analysis, *Res. Rep. 6*, 97 pp., Antarct. Coop. Res. Cent., Hobart, Tasmania, Australia, 1995b.

Rosenberg, M., R. Eriksen, S. Bell, and S. Rintoul, *Aurora Australis* marine science cruise AU9404: Oceanographic field measurements and analysis, *Res. Rep. 8*, 53 pp., Antarct. Coop. Res. Cent., Hobart, Tasmania Australia, 1996.

Rosenberg, M., S. Bray, N. Bindoff, S. Rintoul, N. Johnson, S. Bell, and P. Towler, *Aurora Australis* marine science cruise AU9501, AU9604, and AU9601: Oceanographic field measurements and analysis, inter-cruise comparisons and data quality notes, *Res. Rep. 12*, 150 pp., Antarct. Coop. Res. Cent., Hobart, Tasmania, Australia, 1997.

Schmitz, W. J., On the interbasin-scale thermohaline circulation, *Rev. Geophys.*, *33*, 151–173, 1995.

Schmitz, W. J., On the world ocean circulation: Volume II, the Pacific and Indian Oceans/A global update, *Tech. Rep. WHOI-96-08*, 237 pp., Woods Hole Oceanogr. Inst., Woods Hole, Mass., 1996.

Shum, C. K., et al., Accuracy assessment of recent ocean tide models, *J. Geophys. Res.*, *102*, 25,173–25,194, 1997.

Stammer, D., Steric and wind-induced changes in TOPEX/Poseidon large-scale sea surface topography observations, *J. Geophys. Res.*, *102*, 20,987–21,009, 1997.

Stammer, D., R. Tokmakian, A. Semtner, and C. Wunsch, How well does a 1/4° global circulation model simulate large-scale oceanic observations?, *J. Geophys. Res.*, *101*, 25,779–25,811, 1996.

Stammer, D., C. Wunsch, and R. Ponte, De-aliasing of global high frequency barotropic motions in altimeter observations, *Geophys. Res. Lett.*, *27*, 1175–1178, 2000.

Stevens, D. P., and V. O. Ivchenko, The zonal momentum balance in an eddy-resolving general-circulation model of the Southern Ocean, *Q. J. R. Meteorol. Soc.*, *123*, 929–951, 1997.

Stommel, H., Note on the use of the $T - S$ correlation for dynamic height anomaly computations, *J. Mar. Res.*, *6*, 85–92, 1947.

Stommel, H., A survey of ocean current theory, *Deep Sea Res.*, *4*, 149–184, 1957.

Wang, L., and R. X. Huang, A linear homogeneous model of wind-driven circulation in a β-plane channel, *J. Phys. Oceanogr.*, *25*, 587–603, 1995.

Warren, B. A., J. H. LaCasce, and P. E. Robbins, On the obscurantist physics of 'form drag' in theorizing about the circumpolar current, *J. Phys. Oceanogr.*, *26*, 2297–2301, 1996.

Watts, D. R., C. Sun, and S. R. Rintoul, A two-dimensional Gravest Empirical Mode determined from hydrographic observations in the Subantarctic Front, *J. Phys. Oceanogr.*, *31*, 2186–2209, 2001.

White, W. B., Influence of the Antarctic Circumpolar Wave on Australia precipitation from 1958–1996, *J. Clim.*, *13*, 2125–2141, 2000.

White, W. B., and N. J. Cherry, Influence of the Antarctic Circumpolar Wave upon New Zealand temperature and precipitation during autumn-winter, *J. Clim.*, *12*, 960–976, 1998.

White, W. B., and R. Peterson, An Antarctic Circumpolar Wave in surface pressure, wind, temperature and sea ice extent, *Nature*, *380*, 699–702, 1996.

Whitworth, T., Monitoring the net transport of the Antarctic Circumpolar Current at Drake Passage, *J. Phys. Oceanogr.*, *13*, 2045–2057, 1983.

Whitworth, T., and R. G. Peterson, The volume transport of the Antarctic Circumpolar Current from three-year bottom pressure measurements, *J. Phys. Oceanogr.*, *15*, 810–816, 1985.

Woodworth, P. L., J. M. Vassie, C. W. Hughes, and M. P. Meredith, A test of the ability of TOPEX/Poseidon to monitor flows through the Drake Passage, *J. Geophys. Res.*, *101*, 11,935–11,947, 1996.

S. R. Rintoul, S. Sokolov, and J. Church, CSIRO Marine Research and Antarctic CRC, GPO Box 1538, Hobart, Tasmania 7001, Australia. (steve.rintoul@csiro.au; serguei.sokolov@csiro.au)